Chapter 5. A new phenomenon around circular cylinders

This chapter discusses the experimental evidence at WiSt wind tunnel of a new phenomenon around circular cylinders with a free-end. The peculiar feature is the presence of ring beams along the height of the cylinder. The physical interpretation proposed in this chapter is based on the investigation of pressure measurements through wind tunnel tests.

5.1 Experimental observation

The results of the first set of experiments (April 2011) on the rough circular cylinder without rings in turbulent boundary layer flow (T1-SR0-R1) at several wind tunnel velocities (and thus different Re) represented a good starting point for a deeper investigation (section 4.4). The tests were then repeated by adding 10 equally spaced ring beams along the height of the cylinder in both empty tunnel and turbulent atmospheric boundary layer flow.

Although a certain effect of the ring beams on the flow was expected, it was really surprising to see – immediately, during the first wind tunnel test on the tower with rings – a very interesting phenomenon, which was not just a local effect in the vicinity of the rings. During the experiments, the measurements at WiSt are usually checked and monitored by an oscilloscope, which plots the analogic signal coming out from the amplifiers, and by the computer, which plots on the screen the digitalized raw data. Unusual jumps in the time histories were immediately noted (Figure 5.1).

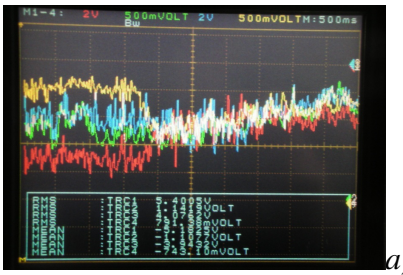
a)

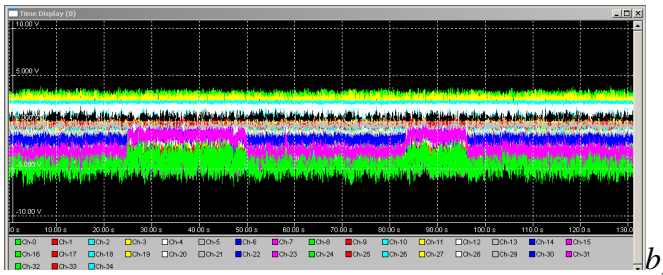
b)

Figure 5.1 Wind tunnel experiments on the circular cylinder with rings: appearance of jumps in the analogic signals (fig. a. oscilloscope) and digital signals (fig. b. computer screen)

The post-processing of the time histories confirmed the presence of jumps at certain points around the circumference. An error during the measurements was at first hypothesized. An error could have occurred at every step in the measurement chain.

However, since the jumps occurred both in the analogic and in the digital signal, if there was an error it could not be in the A/D converter, but before it. Moreover, while the pressure cells AMSYS (type 2) also include the amplifiers, the amplifiers to the pressure sensors Honeywell (type 1) are completely independent from one another (Figure 4.18). Therefore, if there was an error in one of these amplifiers, the others would not be affected. Then, the first check was just to connect a pressure sensor showing the jump to another of these independent amplifiers. This check was repeated several times with different pressure sensors and different amplifiers, but the result did not change. Similarly, it did not seem to be a problem of the connections and of the plastic tubes, because the same test without rings did not show the jump. Therefore, it was decided to go ahead with the measurements because no experimental error could be detected. In addition, the jumps were more evident at angles around 100°-120°, i.e. around separation, so it could have been then reasonable that they were due to a physical cause.

A further proof of validity of the experiments resulted from a closer data inspection. In fact, the jumps were coordinated around the circumference and along the height; they occurred in opposite directions on the two sides of the cylinder and in neighbouring compartments. Furthermore, since the jumps in the time histories occurred mainly at the flanges of the cylinder, they produced jumps in the time histories of the lift, but not in the drag coefficient.

The phenomenon needed to be investigated more deeply and other sets of experiments were planned (section 4.3). This chapter comments on the experimental evidence and reports results of the complete wind tunnel investigation at WiSt laboratory.

The presence of efflux out of the chimney tends to destroy the phenomenon, therefore the undisturbed effect is described in section 5.2 with only reference to the no-efflux condition. The effect of efflux will be mentioned among “other conditions” in section 5.3.5. Moreover, the phenomenon seems to be more related to geometric characteristics of the body rather than to turbulent properties of the flow. In fact, the bistable flow occurs both in empty tunnel (uniform flow) and in atmospheric boundary layer flow. Section 5.2 refers to atmospheric boundary layer flow conditions, the most important ones for the design. A comparative study of uniform and shear flow is addressed in section 5.3.3. A further comparison between different atmospheric boundary layer flows results from the cross-checked investigation at WiSt and CRIACIV wind tunnels (Chapter 6). In fact, the dependency of the bistable flow on the type of atmospheric boundary layer is one of the important issues to be considered in view of the design. First, because the design situation can refer to a different type of

atmospheric boundary layer; secondly, because full-scale properties of strong winds like I_u, shear stresses, integral length scales might be not faithfully reproduced in the wind tunnel. Furthermore, the full-scale condition is associated to higher Re. This is likely the most important point, which is addressed in this chapter as well. The three-dimensionality of the cylinder with a the free-end, the spanwise distance from the tip and the distance between rings - related to the tower diameter - resulted to be key influencing parameters. The slenderness ratio, which was chosen as a fixed parameter in these experiments, should play a role as well (section 5.4), but the investigation of cylinders with different aspect ratios was not possible within this work (Chapter 8).

5.2 Description of a new cross-wind phenomenon

The phenomenon is described in this section with regard to the following condition of experiments: T1-SR1-R1-EF0. Re is $2.5*10^5$ (i.e. tests at 1400 rpm). Further conditions are introduced in the following sections.

5.2.1 Three main features

The occurrence of jumps in the time histories is only one aspect of the phenomenon – perhaps the most evident one – but the analysis of data suggested that three main features describe the flow condition around the circular cylinder with ten rings (Figure 5.3 and Figure 5.4):

1. Bi-stability of the flow: in time, the side pressures jump between two magnitudes;
2. Asymmetric flow around a symmetric structure: on opposite sides of the cylinder, the side pressures jump in opposite directions, so that a lower suction level on one side (e.g. $C_p(100°) \approx -1$) corresponds to a higher suction level on the other side (e.g. $C_p(260°) \approx -1.6$);
3. Spanwise inversion: in adjacent compartments the side pressures jump as well, in opposite directions. For example, if z_1 and z_2 belong to different compartments (e.g. z_1 = 950 mm and z_2 = 850 mm), then $C_p(z_1, 100°) \approx -1$ and $C_p(z_2, 100°) \approx -1.6$ and $C_p(z_1, 260°) \approx -1.6$ and $C_p(z_2, 260°) \approx -1$.

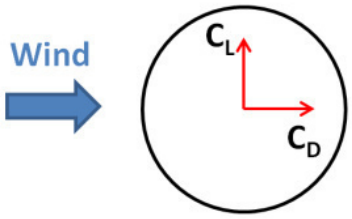

Figure 5.2 Definition of drag and lift coefficients

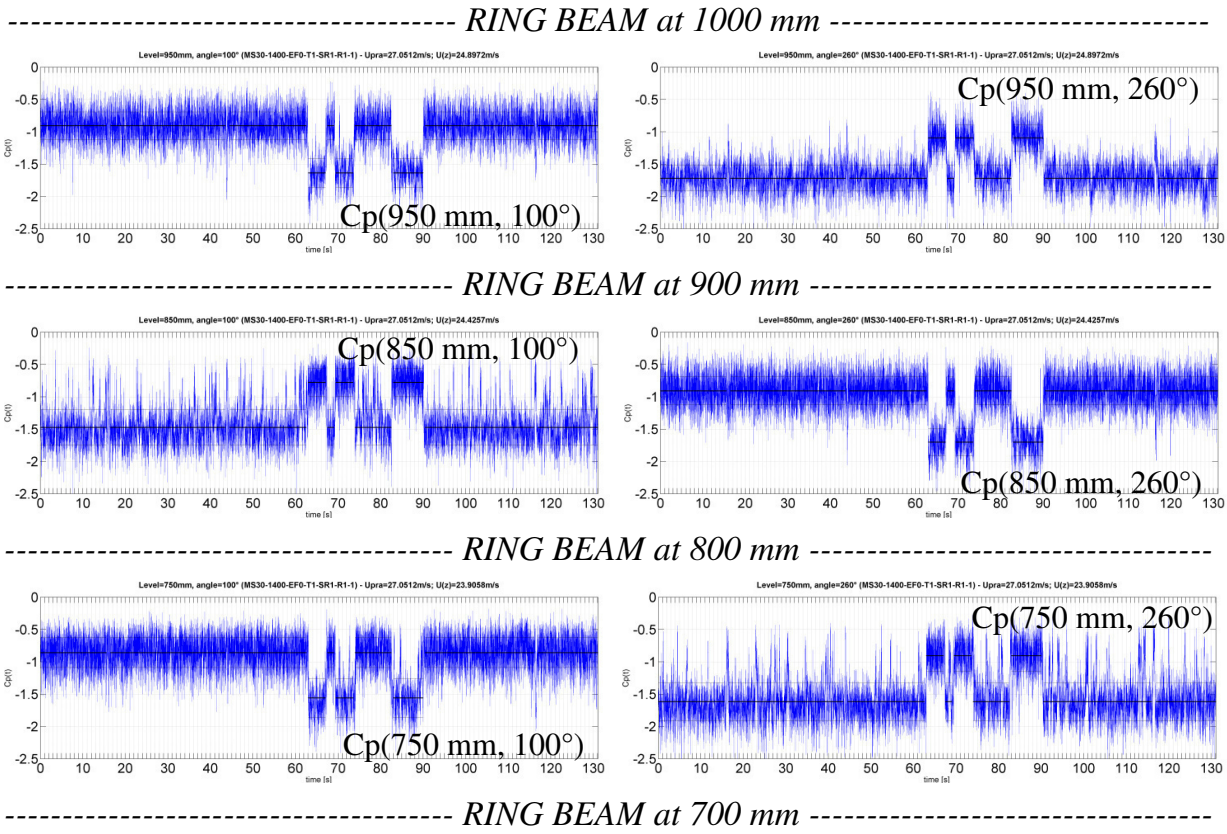

*Figure 5.3 Bistable and asymmetric flow with spanwise inversion. Time histories of C_p at: 950-850-750 mm, 100° and 260° (WiSt, T1-SR1-EF0-R1, Re = 2.5*10^5)*

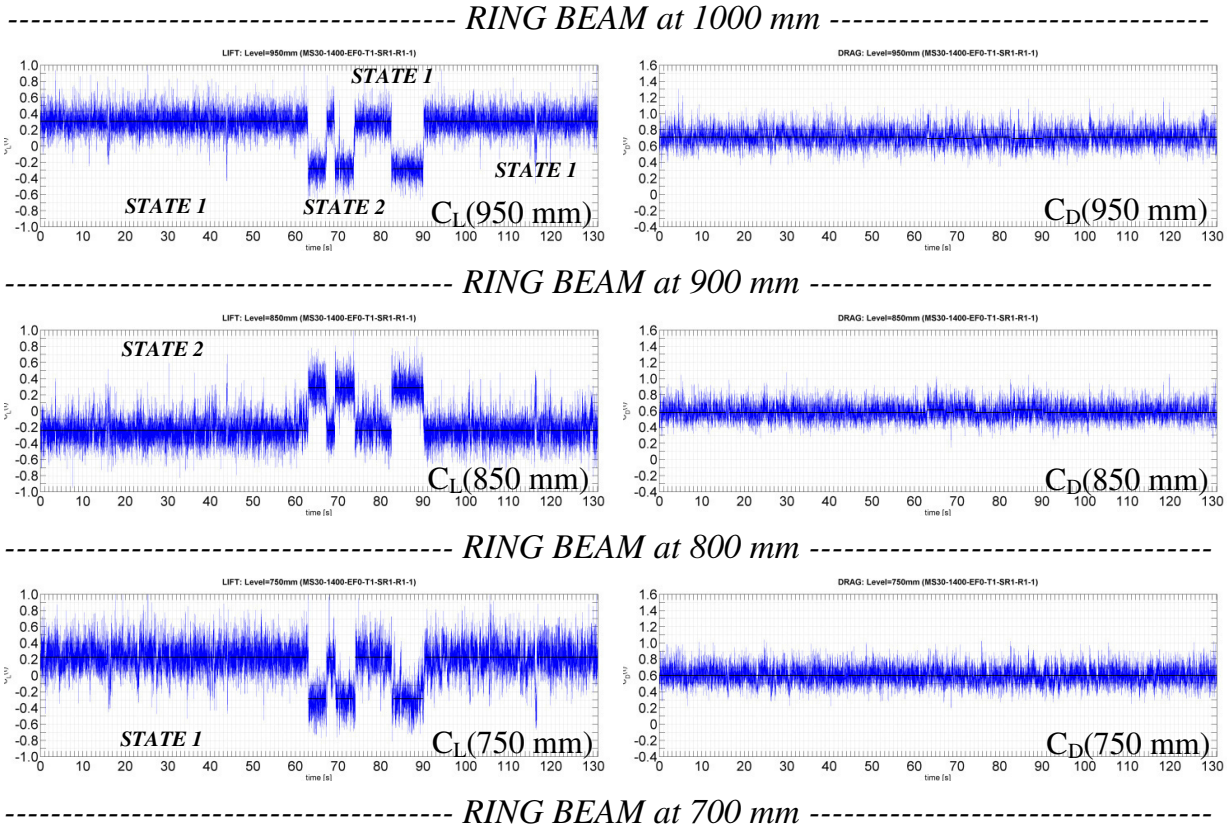

*Figure 5.4 Time histories of C_L and C_D at 950-850-750 mm (WiSt, T1-SR1-EF0-R1, Re = 2.5*10^5)*

The phenomenon continues along the height of the tower, but at low levels (z < 0.6H) the mixture between the two states is more pronounced. The progressive disruption of the bistable flow along the height, as the distance from the tip increases, is an issue addressed in Chapter 6.

The mean and the rms values of the time histories are calculated separately for each interval of time before and after a jump; their circumferential distribution proves that two states can be detected. They are asymmetric but identical, just mirrored (Figure 5.5 and Figure 5.6, z/H = 0.75). Because of that, the flow is called bi-stable. As a consequence of the asymmetry, that is created by higher suction on one side of the cylinder, the mean lift coefficient is not zero (Figure 5.4). Depending on the interval of time which is considered, the mean lift can be either positive or negative. For convention, the "state 1" identifies the intervals of time associated to positive mean lift and the "state 2" is associated to negative mean lift. In the reference system of the wind tunnel, being the x-axis along the wind tunnel and the y-axis in the across wind direction (see the Drawing 1 on page 103), the state 1 has the high-suction side between 180° and 360°.

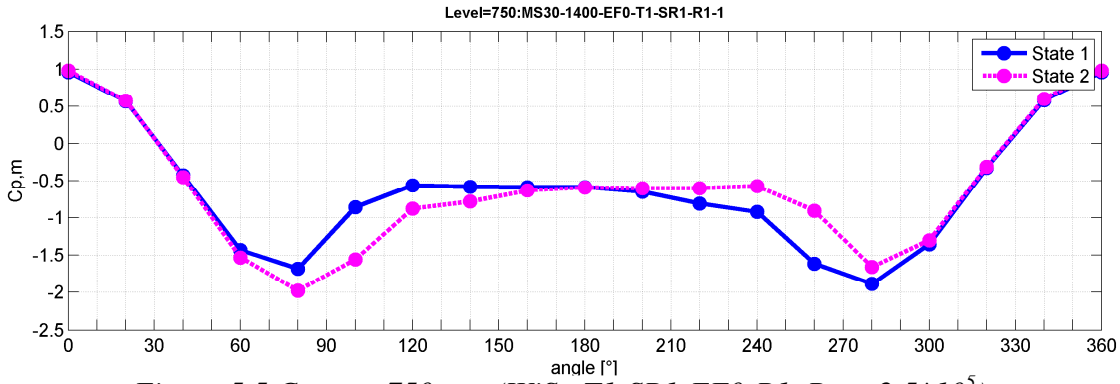

*Figure 5.5 Cp,m at 750 mm (WiSt, T1-SR1-EF0-R1, Re = 2.5*10^5)*

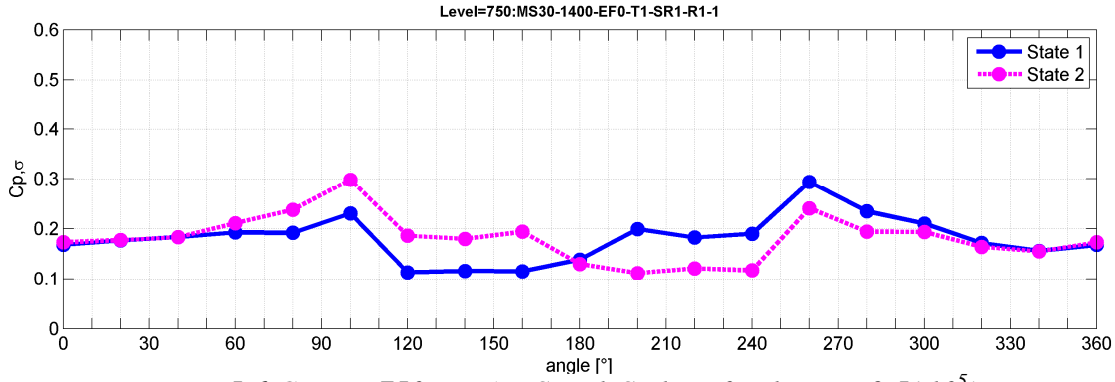

*Figure 5.6 Cp,σ at 750 mm (WiSt, T1-SR1-EF0-R1, Re = 2.5*10^5)*

The state 1 at z/H = 0.75 is now analyzed in more detail in Figure 5.7 ($C_{p,m}$) and Figure 5.8 ($C_{p,\sigma}$). The asymmetric pressure distributions are fitted with spline curves. It can be seen that the higher suction on one side only of the cylinder is associated to a

rearward movement of the separation point ($\varphi_N \approx 240°$ in Figure 5.7) and a complicated flow structure in the wake. Usually, the recirculation region in the wake of a cylinder between the separated shear layers is characterized by random fluctuations; they are not relevant for the structural design, but the wake structure is of great interest from the fluid-dynamic point of view. In particular, in presence of 10 ring beams along the tower, a recirculation bubble can be detected in the mean and rms pressure distributions. In fact, between 240° and 200°, i.e. after separation on the high-suction side, the mean pressure distribution presents a horizontal step at the constant value ≈-0.8 and then it rises again until ≈-0.6, which remains constant in the rest of the wake, also on the other side of the cylinder (low-suction side). The presence of such a horizontal step after separation can be attributed to a reattachment of the separated shear layer and further separation (Zdravkovich, 1997, page 166), i.e. the formation of a separation bubble. In the range 240° and 200° the rms values undergo a horizontal step as well, at a rather high value (Figure 5.8): the value is, in fact, comparable to the fluctuations at stagnation, while fluctuations in the wake should normally have a standard deviation about one half of the ones at stagnation (as it is in the wake on the low-suction side of the cylinder). Because of that, in case of rings the two sides of the cylinder are named “normal side” and “bubble side”, i.e. “low-suction side” and “high-suction side”, respectively.

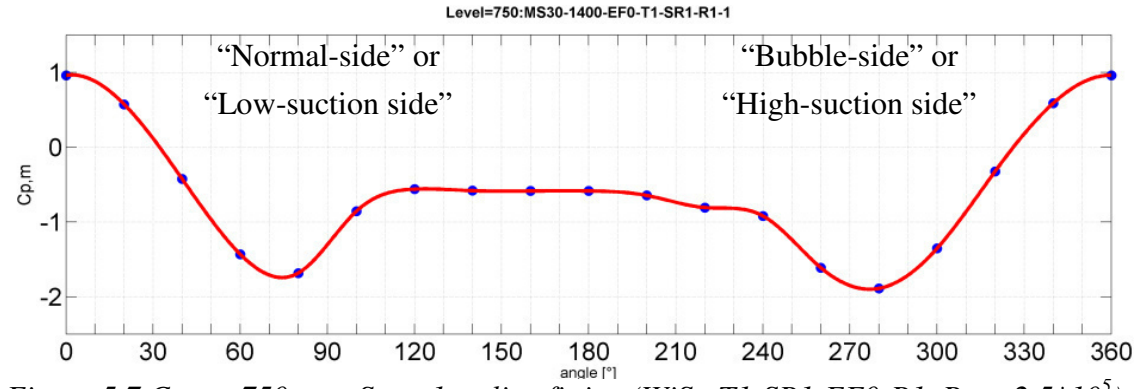

*Figure 5.7 $C_{p,m}$ at 750 mm. State 1, spline fitting (WiSt, T1-SR1-EF0-R1, Re = 2.5*10^5)*

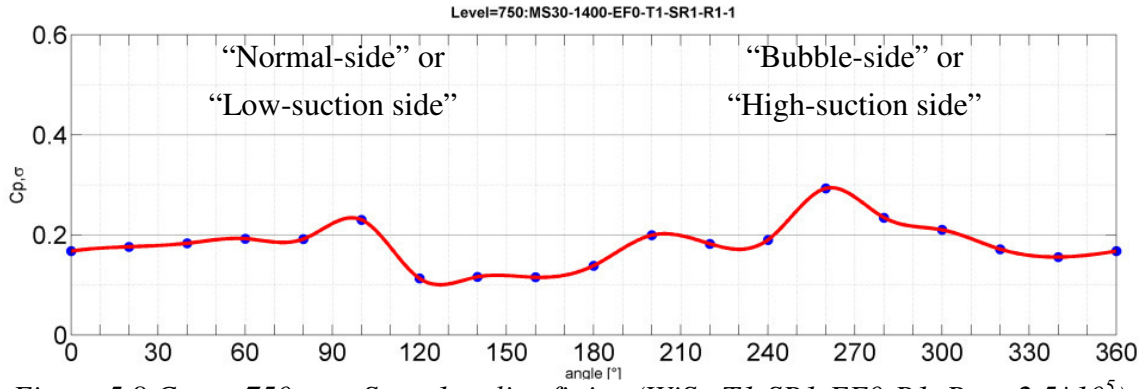

*Figure 5.8 $C_{p,\sigma}$ at 750 mm. State 1, spline fitting (WiSt, T1-SR1-EF0-R1, Re = 2.5*10^5)*

Another peculiar feature is the spanwise inversion along the height of the cylinder, which means that the state of the flow is alternated in neighboring compartments. In fact, Figure 5.4 proves that during each stable interval of time the mean lift coefficient changes its sign in neighboring compartments, so that the steady cross-wind force changes its versus along the height of the cylinder. This is due to the vertical alternation of high- and low-suction sides of the cylinder, as shown in a transversal view in Figure 5.9.

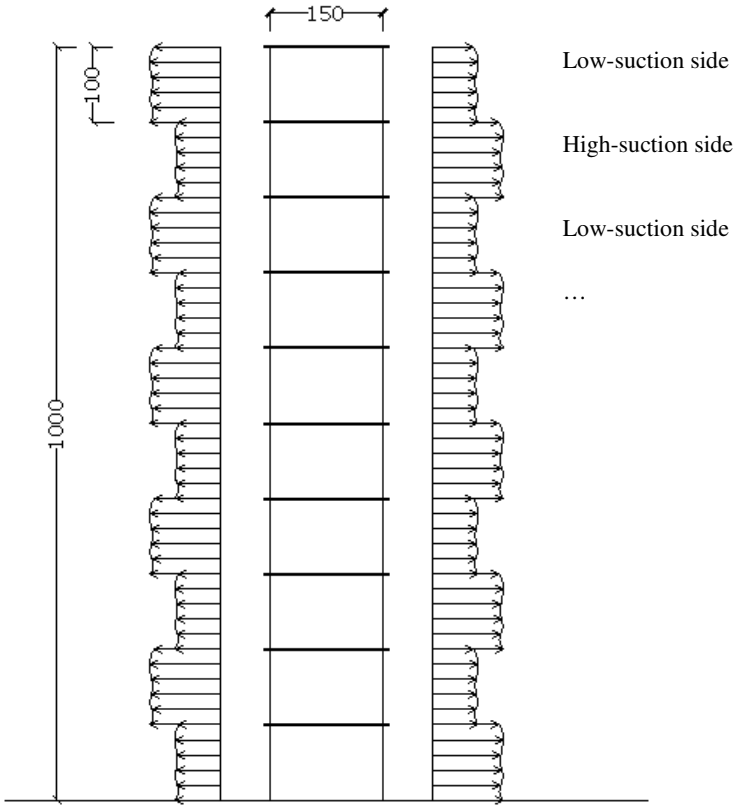

Figure 5.9 Spanwise inversion: high-suction and low-suction sides, transversal view.

5.2.2 Step by step through a jump between two states

The jump between the two states of the bistable flow is accompanied by a significant displacement of the stagnation point and the formation of a bigger separation bubble, which suddenly seems to move in the wake on the other side of the cylinder. This can be seen in a sequence of instantaneous pressure distributions within a jump. In particular, 8 significant time steps are highlighted in Figure 5.10, when the lift is either maximum or minimum in the vortex shedding cycle and crossing zero before changing state. The x-axis in the figure plots the number of time steps, it is remembered that the sampling frequency is 2000 Hz, therefore the figure plots a time window of 2 seconds.

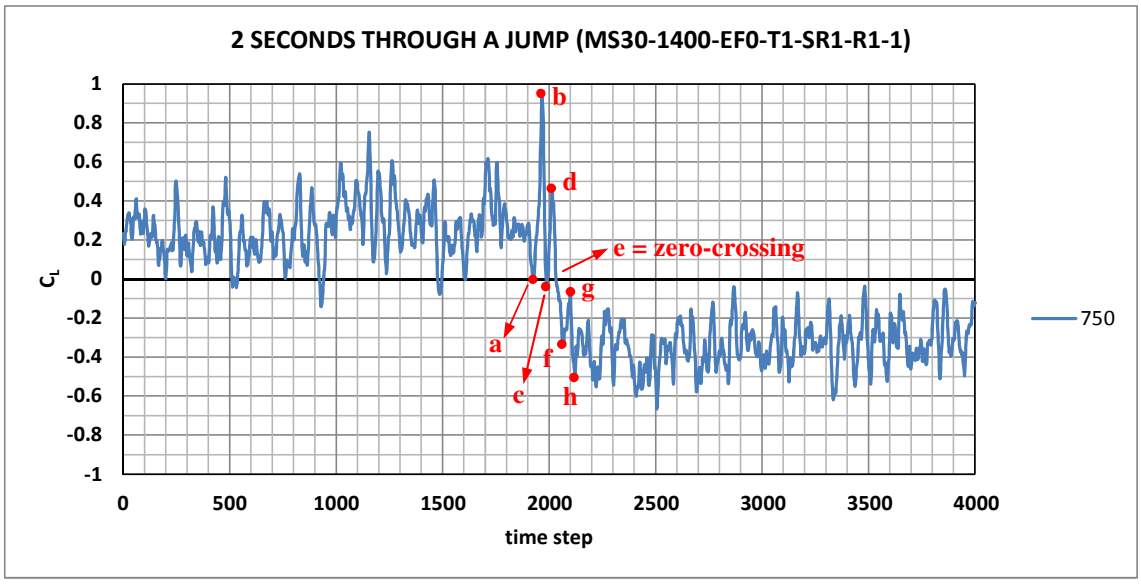

*Figure 5.10 2s-time history at 750 mm ($n_{sampling}$ = 2000 Hz) : transition from state 1 to state 2 (WiSt, T1-SR1, Re = 2.5*10^5)*

Figure 5.11 (a-d) plots instantaneous distributions in the state 1, i.e. the state of positive mean lift. Then, in figure e) the flow is changing state and after that the instantaneous distributions belong to the state 2 (figures f-g-h).

In the state 1, during a shedding cycle the lift oscillates between a minimum value which is close to zero and a maximum positive value which corresponds to a von Karman vortex shed on the bubble side. For example, in Figure 5.11a) the instantaneous pressure distribution results to be almost symmetric. In fact, the lift at those instants is around the minimum value because the vortex is shed on the normal side, where the mean lateral suction is lower than on the bubble side. Thus, the growth of the vortex on the normal side reduces the asymmetry. Instead, when the vortex is shed on the bubble side, the lift assumes an extreme value, which is either positive (state 1) or negative (state 2). In the compartment below the ring the situation is simultaneously reversed.

At some time, there might be the formation of a bigger bubble (Figure 5.11d), which is anticipated by a displacement of the stagnation point. Such a displacement occurs on the same side of the cylinder at diffetent levels (despite the spanwise inversion of lift) and it is sligthly anticipated at higher levels, so that the transition of state at 950 mm appears to be about 0.11 seconds (in the wind tunnel time scale) earlier than 20 cm below. This is a very short time in the wind tunnel, but it is remembered that the vortex shedding period is more than three times shorter (S_tU/D) ≈ 0.2*25/0.15 = 0.03s.

After the zero crossing (Figure 5.11e) the state has changed and a separation bubble of smaller size (comparable with the one in the mean distribution, plotted in Figure 5.11) develops on the other side of the cylinder.

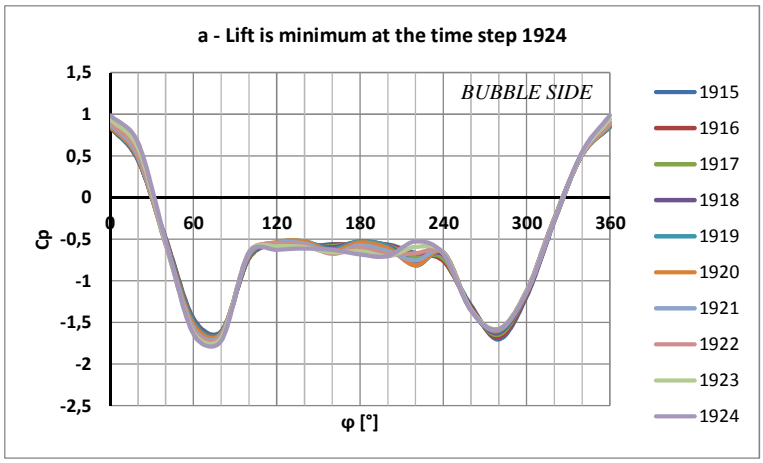

Figure 5.11 a) State 1; n. 1924 in the legend is the time step "a" in Figure 5.10

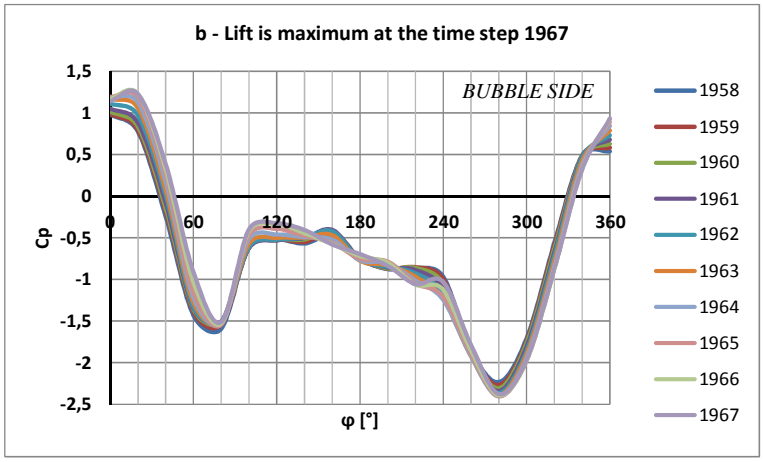

Figure 5.11 b) State 1; n. 1967 in the legend is the time step "b" in Figure 5.10

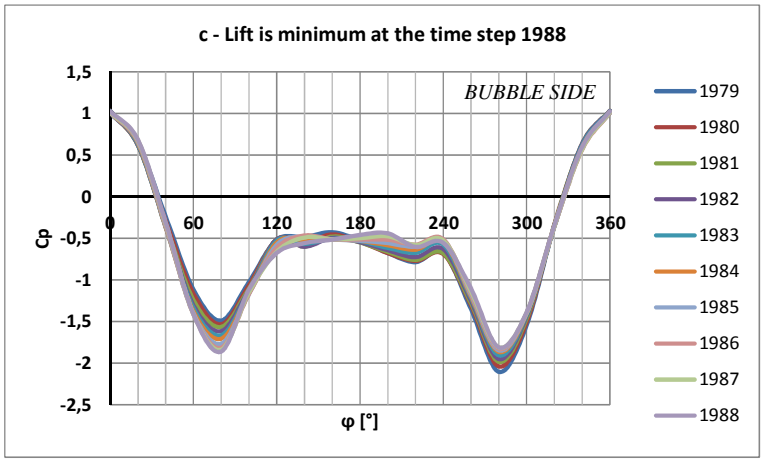

Figure 5.11 c) State 1; n. 1988 in the legend is the time step "c" in Figure 5.10

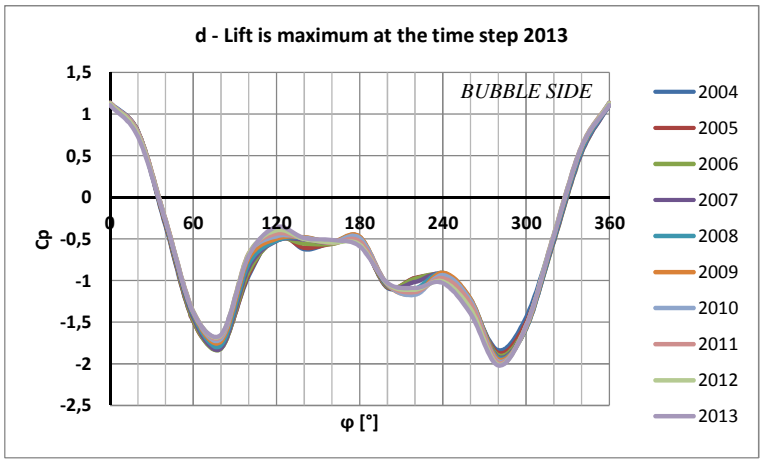

Figure 5.11 d) State 1; n. 2013 in the legend is the time step "d" in Figure 5.10

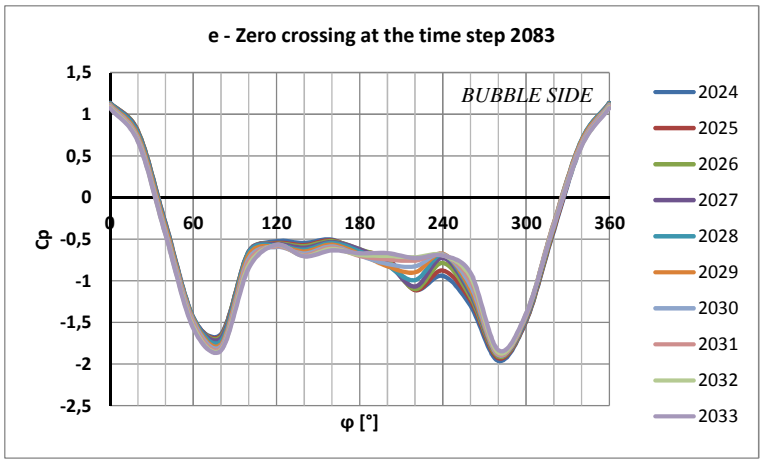

Figure 5.11 e) Change of state; n. 2033 in the legend is the time step "e" in Figure 5.10

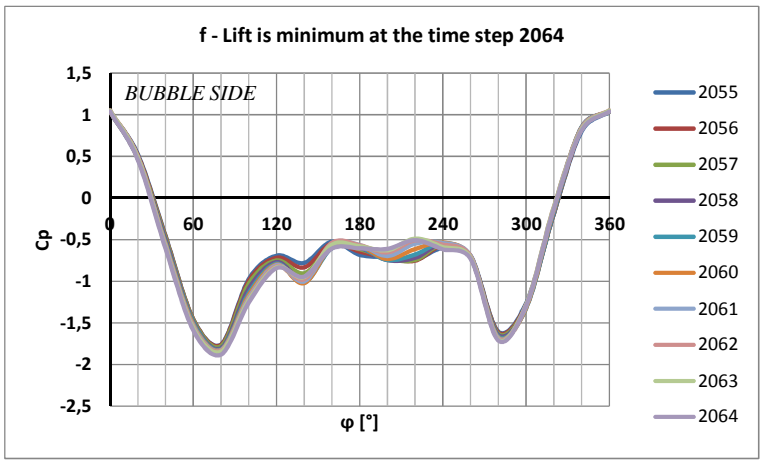

Figure 5.11 f) State 2; n. 2064 in the legend is the time step "f" in Figure 5.10

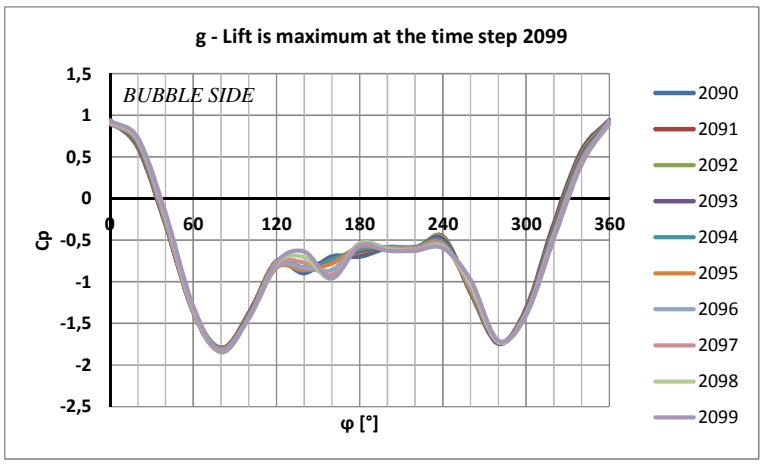

Figure 5.11 g) State 2; n. 2099 in the legend is the time step "g" in Figure 5.10

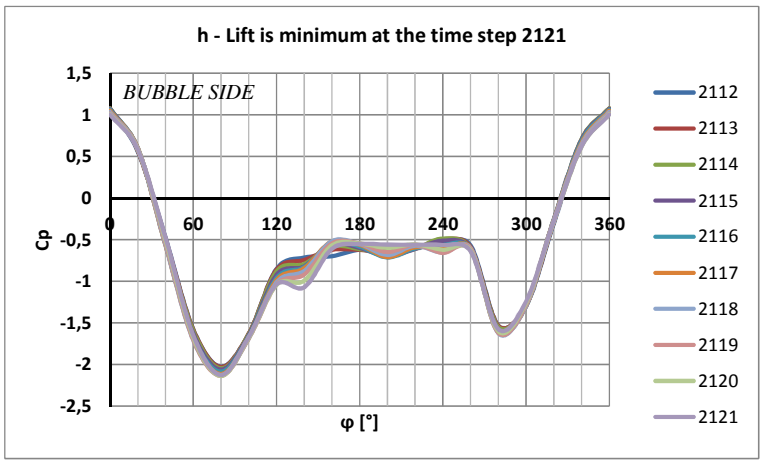

Figure 5.11 h) State 2; n. 2121 in the legend is the time step "h" in Figure 5.10

Figure 5.11 a-h) Momentary distributions during a jump (10 time steps = 10/2000 s), Re = $2.5*10^5$

5.2.3 Literature and novelty

The asymmetry of the pressure distribution created by the rings is associated to higher suction and formation of a separation bubble on one side only of the cylinder. This phenomenon might be - in itself - not new. A similar effect is well-known around circular cylinders (without rings) in the critical range of Re, as mentioned in Chapter 3. However, the conditions of occurrence (further discussed in section 5.3) of the bistable phenomenon evidenced in this Dissertation make it original and physically unique.

The similar case reported in literature (Figure 3.2) is very sensitive to Re and occurs in a small range of Re just before the critical value. Moreover, it is also sensitive to disturbances and perturbations in the flow (such as turbulence). The phenomenon is thus observed only in smooth flow on smooth cylinders. It is also very difficult to catch it. The physical reason which produces the separation bubble is strictly related to the Reynolds number, because it governs the transition from laminar to turbulent flow. In particular, the flow is asymmetric because such a transition has occurred in the shear layer after separation (laminar separation) on one side only of the cylinder. On that side where transition occurred the turbulent flow gets more energy and is able to reattach. The second separation is then turbulent. In between, there is the formation of a separation bubble, namely laminar separation bubble. Transition from laminar to turbulent flow, which occurs after the first laminar separation, is due to some random perturbations on that side of the cylinder. Therefore, in ideal conditions, the side on which it may occur is completely random. Moreover, it can occur on one side only of the cylinder only if there is a low probability that there are perturbations on the two sides able to initiate a transition to turbulent flow. Because of that, the asymmetric phenomenon disappears in turbulent flow and/or on a rough cylinder: perturbations and laminar separation bubbles likely develop on the two sides of the cylinder and that is the critical (symmetric) state.

In the present case of study, the incoming flow is turbulent and the cylinder is rough. In the pictures shown up to now the wind tunnel is at full-speed ($Re \approx 2.5*10^5$, effective Re about one order of magnitude higher). In these conditions, laminar separation can be absolutely excluded. In fact, transition from laminar to turbulent boundary layer should occur very close to stagnation and certainly before separation. Consequently, even though the higher suction on one side of the cylinder may suggest the existence of a separation bubble, like in the well-known bistable flow in the critical range of Re, it cannot be a separation bubble in the classical sense, i.e. a laminar separation bubble. A laminar separation bubble is caused by a physical reason, that is transition to turbulent conditions in the free-shear layer after separation and

consequent reattachment. As the formation of the laminar separation bubble is excluded in the conditions of the experiments, the corresponding physical explanation fails. For the same reason, the high sensitivity of the laminar separation bubble to Re, to the surface roughness of the cylinder and to the turbulence of the incoming flow should not necessarily be confirmed in the present phenomenon. In fact, it is not. It should also be remembered that the result shown up to now in this chapter occurs in a state of the flow far beyond the critical drop ($Re = 2.5*10^5$, surface roughness R1), as confirmed by Figure 4.29. Thus, although the dependency on Re is an issue which deserves particular attention, it is clear that it cannot be just an effect of Re_{cr}.

What is completely new is also the spanwise variation of the asymmetry. In the well-known case of literature, Bearman (1961) observed that "the distribution of base pressure along the span suggested that the establishment of a bubble on one side takes place along the complete length of the cylinder and this was later confirmed by surface oil flow patterns". In absence of ring beams along the height, in fact, there is no reason for a spanwise inversion. It is a peculiar effect of the compartments created by the rings. In particular, it must be a result of the interaction between compartments. The alternation along the height of higher and lower side pressures determines vertical pressure gradients and thus flow movements between different levels. It is believed that the key is in the recirculation bubbles in the near wake of the cylinder.

The occurrence of jumps between the two states does not present regularity. The random nature is, in any case, not surprising. It is typical, for example, of side-by-side cylinders. It reflects the random nature of the turbulent flow. Also the bistable flow in the critical range of Re presents the same characteristic: a random perturbation in the flow, on either side of the cylinder, may initiate the phenomenon.

What is interesting, moreover, is the stable nature within each state. After being initiated, a certain state establishes. This is completely different from the unsteadiness of vortex shedding, where cross-wind oscillations of the lift force average to zero. From the experiments, it was not straightforward to infer that symmetric conditions can be achieved by averaging on an infinitely long period. In any case, an infinitely long period cannot be justified in the design of a structure during a wind storm. But it must be remembered that the stable nature of the asymmetric condition is a peculiar feature of the well-known bistable flow of literature, too. The name itself, bi-stable flow, highlights that we are dealing with two conditions of stability, not with instability. In the case of literature, Schewe (1983) wrote "the immediate formation of a one-sided bubble leads to steady circulation around the cylinder. This effect results in acceleration of the fluid on the side where the boundary layer transition has

occurred and in deceleration at the other side of the cylinder. Deceleration of the fluid delays the transition in this detached boundary layer and hence the formation of the bubble. This coupled occurrence of the development of a bubble on one side with the deceleration of the fluid on the other side (i.e. decrease in the Reynolds number of this boundary layer) probably causes stabilizing and fixing of the asymmetric flow state". Acceleration of the flow on the bubble side is related, in a phenomenon which is highly sensitive to Reynolds effects, to the Reynolds number. Again, the reason here must be profoundly different, but the effect is the same.

The interesting debate between known and unknown, literature and novelty, motivated further investigation of the phenomenon and a proper revision of the wind tunnel experiments. It seemed worthwhile to go deeper in the study by testing different situations. The crucial question is not only the physical reason which produces the asymmetric and bistable effect, but also the systematic investigation of the conditions of occurrence and their dependency on the Re, i.e. on the wind tunnel scale. The two wind tunnels available for the experiments allowed to test only a limited range of Re, so that surface roughness was introduced to increase the effective range. Several different combinations of wind velocities and rib height and distributions were tested. Section 5.3 explains the details, but it is now anticipated the surprising result that the phenomenon seems to stabilize even more as Re increases. Further experiments at higher Re (like full-scale conditions) would require higher velocities and bigger wind tunnels (or pressurized flow); they would be much more expensive, but rather decisive. Fluid dynamic simulations (section 6.3) were performed in parallel to the last part of the experimental work (in CRIACIV) also with the aim to explore higher Re.

5.3 Conditions of occurrence

In order to accept and be convinced of the new experimental phenomenon, it has been tested with regard to the following conditions of occurrence: [1)] different wind tunnel velocities (thus different Reynolds numbers); [2)] different surface roughness on the model, in terms of height and distribution of ribs; [3)] different boundary layers (uniform and shear flow); [4)] removal of hypothesized experimental unintentional disturbances. The tests were also repeated in presence of [5)] efflux. Then, a further question that was addressed regarded the sensitivity of the phenomenon to [6)] different design choices, for example with a different number of ring beams (5 or 7) and with smaller rings (whose width is halved).

This sensitivity analysis has been performed in only one wind tunnel (WiSt laboratory) and mostly in turbulent boundary layer flow. Only the most representative tests were

repeated at CRIACIV for further validation in a different laboratory (Chapter 6). The results in WiSt tunnel are reported in the following. However, the sensitivity analysis with 10 rings did not suggest any reason for which the phenomenon should not be expected. The phenomenon is in any case mitigated by the presence of efflux and by using fewer and/or smaller rings.

Although the sensitivity analysis was carried out with the purpose of being as much general as possible, the tower model and the experimental set-up limited the experimental investigation to the 3D condition (cylinder of finite length with a free-end) and H/D = 6.7, as well as to a certain range of Re. Tests in two-dimensional flow and with different slenderness ratios would be recommended for future investigation, as well as tests with a different distribution of rings (Chapter 8). The load and response calculation (Chapter 7) should give an indication about the importance of additional experimental investigation in the structural design of Solar Updraft Towers. It basically depends on the level of structural optimization one wants to achieve.

5.3.1 Dependency on the Reynolds number

The dependency of the phenomenon on the Reynolds number is at first studied for a certain surface roughness by varying the wind tunnel velocity. The preliminary investigation described in section 4.4.3 showed that the best target condition, in terms of effective Reynolds number, is achieved by using the surface roughness condition R1. It is then the reference condition through the whole dissertation and also in this sub-section 5.3.1. In any case, the tests were also repeated with different surface roughness, in order to study its effect. The most representative results are reported in section 5.3.2.

As described in Chapter 4, five levels of wind velocity in the working range of the wind tunnel at WiSt were selected for most tests: 600-800-1000-1250-1400 rpm (corresponding to $U_{pra} \approx$ 12-16-20-25-27 m/s, respectively). Lower wind speeds (up to 3 m/s) were only tested on the smooth cylinder to reach the subcritical range (section 4.4.3).

Figure 5.12 plots the results versus Re at z = 950 mm in the two states, which can be considered reasonably equal. The dependency of the drag coefficient on Re is less pronounced than in SR0, at Re_{cr} there is only a small drop. The interesting and peculiar feature of the phenomenon is the presence of a mean steady lift throughout the whole tested range of Re. It does not show any tendency to disappear at higher Re. Because of that, so far (on the basis of these experiments) it is not expected any disappearance of the phenomenon at higher Re. The rms values in the two states do not show a significant dependence on Re.

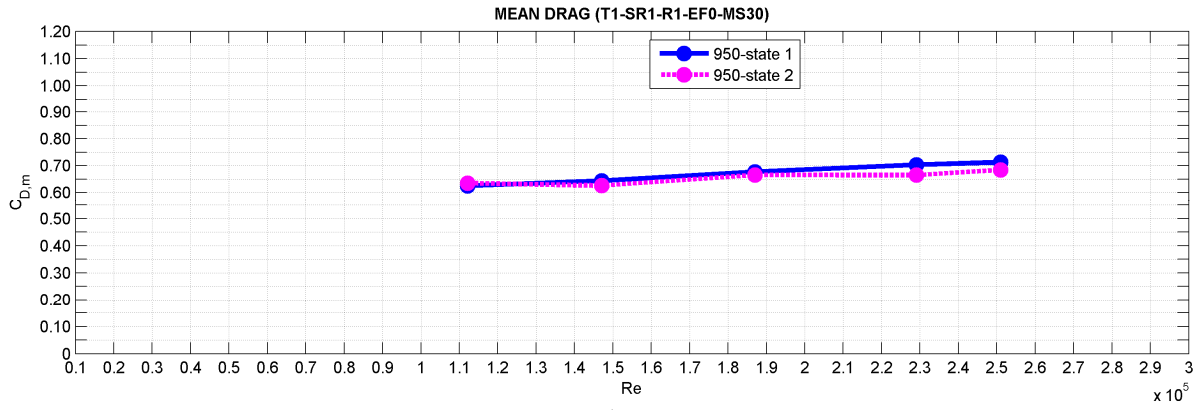

a)

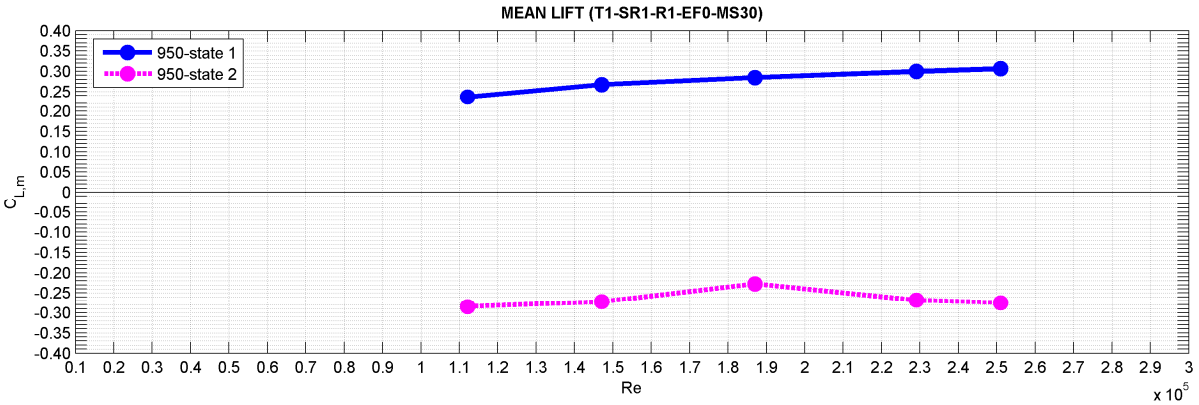

b)

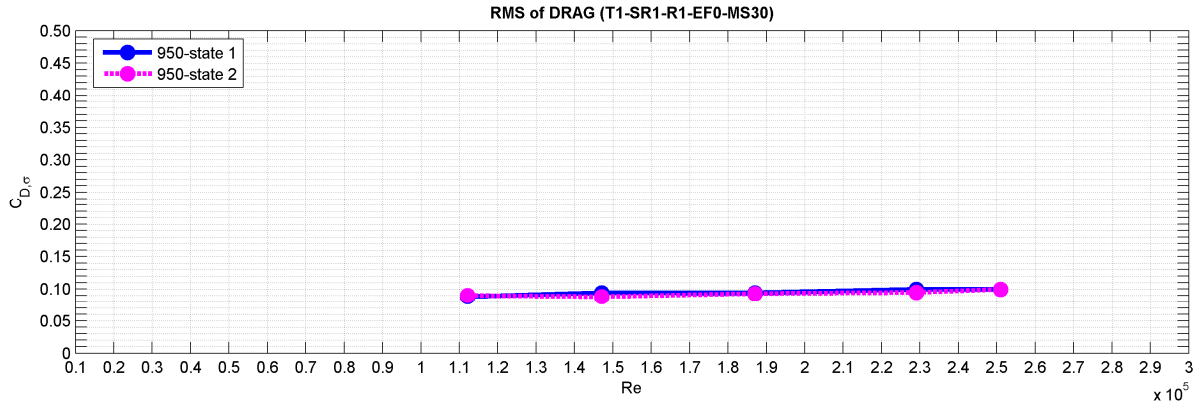

c)

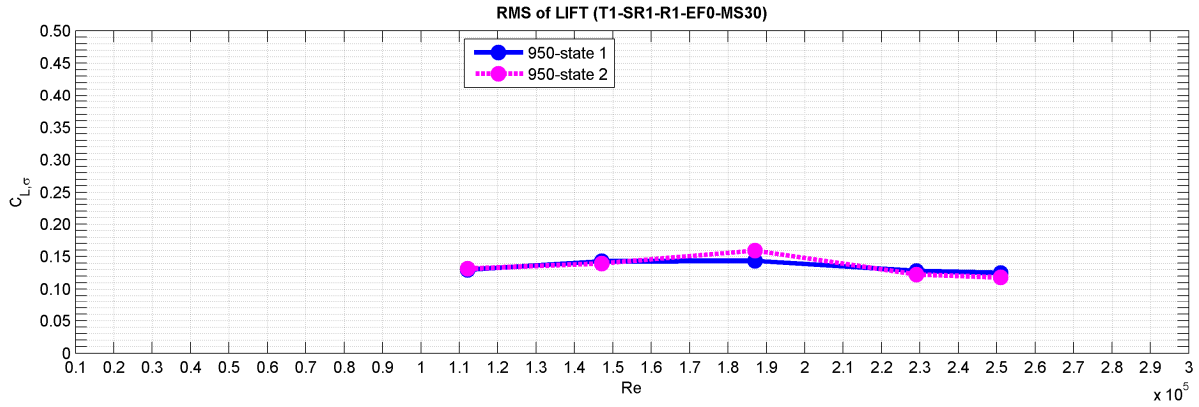

d)

Figure 5.12 a-d) Bistable and asymmetric flow within one state as a function of Re at 950 mm: a) $C_{D,m}$; b) $C_{L,m}$; c) $C_{D,\sigma}$; d) $C_{L,\sigma}$ (WiSt, T1-SR1-R1-EF0)

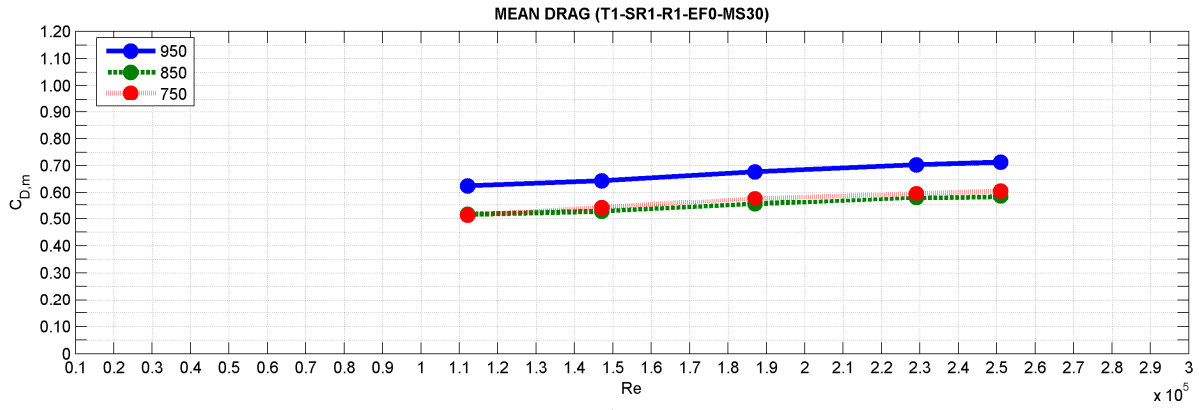

a)

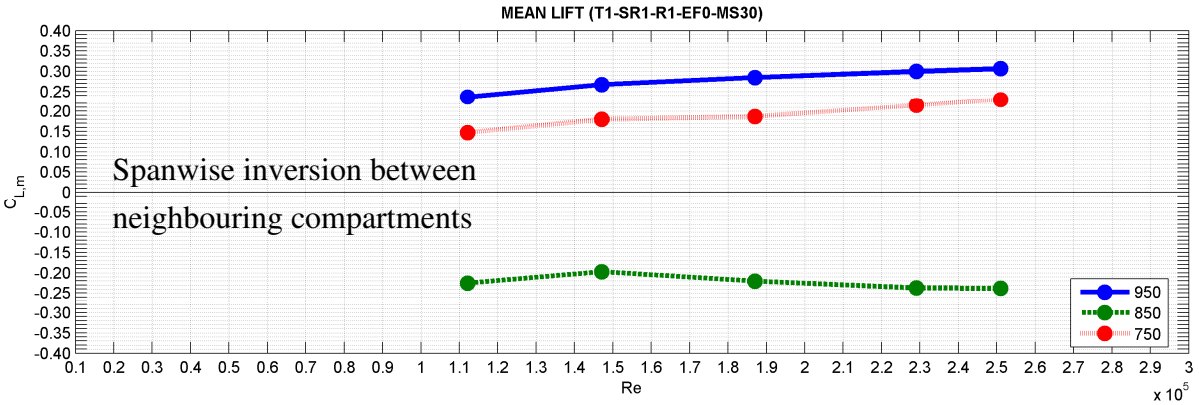

b)

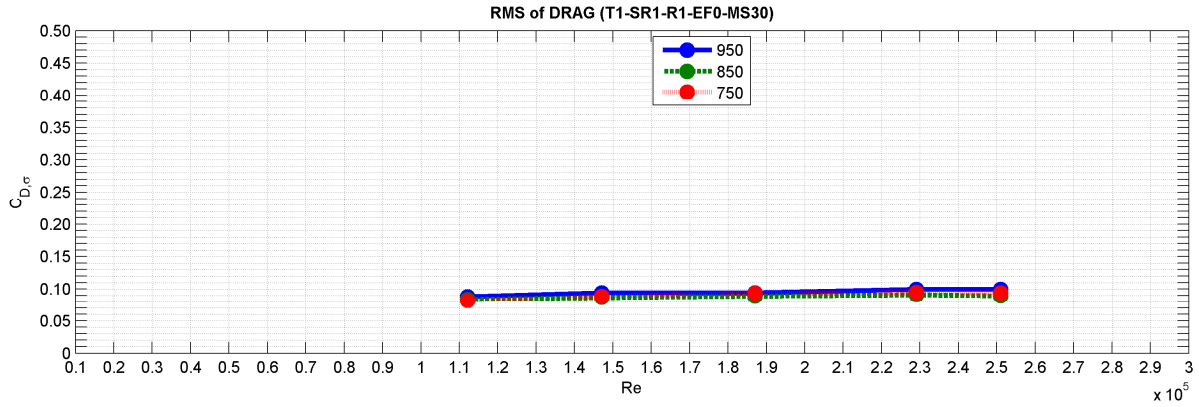

c)

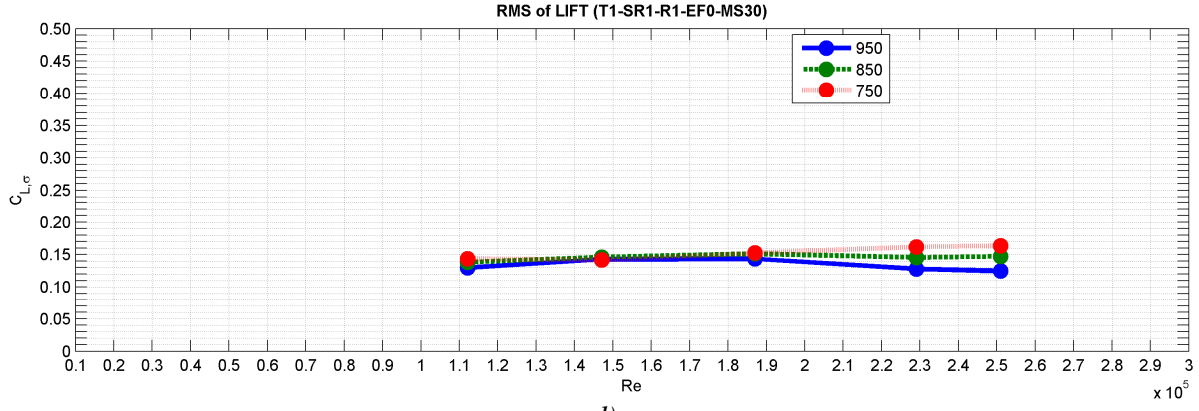

d)

Figure 5.13 a-d) Bistable and asymmetric flow within one state as a function of Re at 950-850-750 mm: $C_{D,m}$, $C_{L,m}$, $C_{D,\sigma}$, $C_{L,\sigma}$ (WiSt, T1-SR1-R1-EF0)

Figure 5.13 shows the dependency of the phenomenon on the height in the tip region (the situation at lower levels is explained in Chapter 6). Only one of the two states is considered. Due to the spanwise inversion, the mean steady lift alternates in sign between different compartments. This is a very peculiar feature of the phenomenon. It can also be observed that the tip effect is not so pronounced and, apart from the highest level (950 mm), the mean drag stabilizes on the same value. The rms values do not show significant dependency on height.

Figure 5.14 plots the mean pressure coefficients distributions at different Re and explains the weak dependency of the force coefficients on Re. On the normal side of the cylinder (0-180°), as the wind velocity increases, the lateral suction decreases and the separation point moves upstream (such a movement is maybe concealed by the linear interpolation in the figure). This is typical of the supercritical range on a rough cylinder (Figure 3.8). The suction in the wake tends to increase, but this is especially appreciable on the bubble side, where lateral suction remains high. Because of that, as Re increases, the asymmetric condition tends to stabilize.

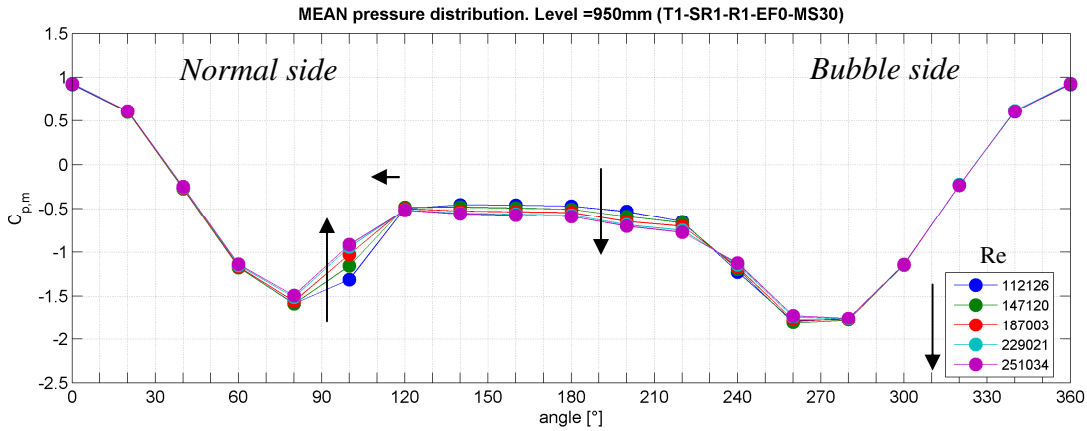

Figure 5.14 Bistable and asymmetric flow as a function of Re at 950 mm: $C_{p,m}$ in state 1 (WiSt, T1-SR1-R1-EF0)

5.3.2 Effect of surface roughness

Surface roughness, consisting of ribs, has a very strong effect on the flow because it changes the effective Reynolds number. As a consequence, it has an effect on the pressures, both with and without rings.

The most suitable flow condition for the design of the solar tower is achieved in the wind tunnel by using surface roughness R1, as already discussed in Chapter 4, whose result have been already presented (also in presence of rings, see section 5.2).

It is not in the purpose of this section to discuss the effect of a different state of the flow (produced by a different flow velocity and/or a different type of surface

roughness) on the bistable phenomenon, because it would not be relevant for the design of solar updraft towers. The aim of this section is to exclude that the occurrence of the bistable phenomenon may only be a matter of a certain choice – for experimental purposes – of surface roughness for the wind tunnel model. Thus, some tests were done by applying 10 rings in the following conditions: surface roughness R1, R2, R3, R4, R5 at 600, 800, 1000, 1250, 1400 rpm and on the smooth cylinder (R0) at 100, 200, 400, 600, 800, 1000, 1250, 1400.

Out of all the tests, the main result that can exclude that the ribs are responsible for creating the bistable flow is plotted in Figure 5.15. It has been measured on the smooth cylinder at low velocity (200 rpm, ≈ 5 m/s) in turbulent boundary layer flow. The state of the flow is at the very end of the subcritical state. The figure shows that the jumps in the time histories still occur and the histogram of the pressure coefficient highlights the bistability, even without ribs, even in a different state of the flow. The angle 100° at 950 mm is chosen as representative in the picture.

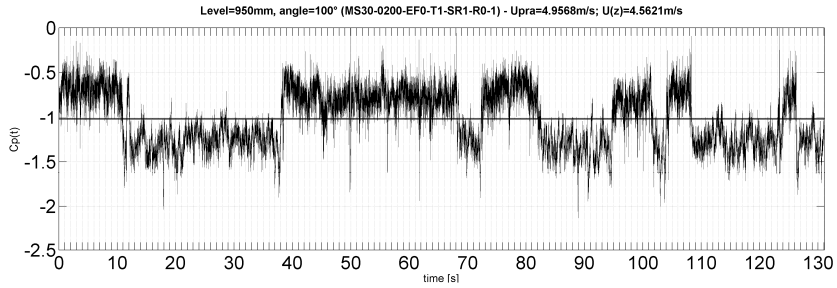

Figure 5.15 Bistable flow on the smooth cylinder (R0) with 10 rings (U_{pra} ≈ 5 m/s = 200 rpm): C_p(950m,100°) (WiSt, T1-SR1-R0-EF0)

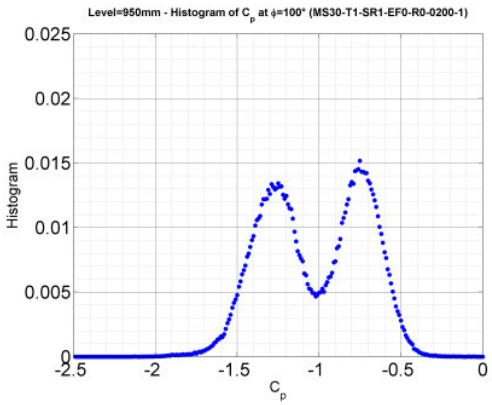

Figure 5.16 Histogram of C_p (time history in Figure 5.15)

Figure 5.17 is an example which shows that jumps in the time history also occur in a different surface roughness condition. In this example, higher roughness (R3) has been applied and the wind tunnel velocity is 800 rpm. This condition presents the same $C_{D,m}$ and pressure recovery as R1-1400rpm (section 4.4.3).

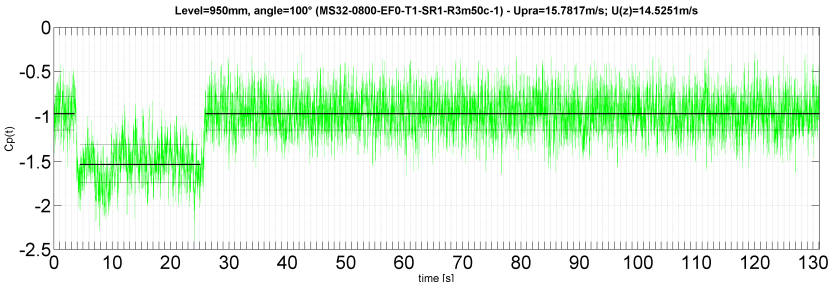

Figure 5.17 Bistable flow on a rougher (R3) cylinder with 10 rings ($U_{pra} \approx 16$ m/s = 800 rpm): C_p(950m,100°), (WiSt, T1-SR1-R3-EF0)

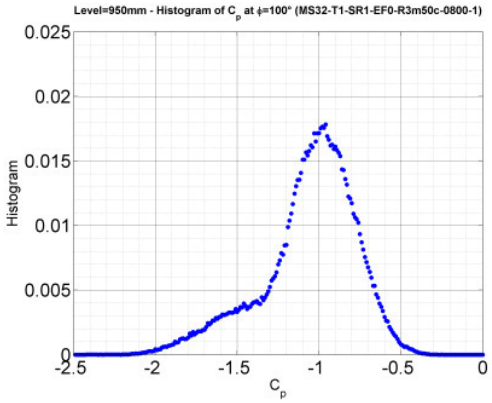

Figure 5.18 Histogram of C_p (time history in Figure 5.17)

5.3.3 **Influence of boundary layer**

The bistable flow occurs both in shear and in uniform flow. The values of the turbulence intensity and of the integral scales are not the governing parameter of the phenomenon, because the uniform and the shear boundary layer flow in WiSt (T1 and T3), as well as shear boundary layer in CRIACIV, are characterized by very different parameters (sections 4.1 and 6.1) and this does not prevent the occurrence of the phenomenon in the tip region. In fact, the phenomenon appears in the three cases. However, as it will be better explained in Chapter 6, the bistable flow tends to become a mixture of the two states at lower levels and there is a height at which the asymmetric flow starts to vanish. In particular, this disruption of the phenomenon starts at a certain level along the tower as a more rapid alternation of jumps on one side of the cylinder, that is the bubble side at that level.

Being the bistable flow a three-dimensional effect, it is basically governed by the free-end and the highest compartment, therefore it should not be surprising that the effect tends to disappear as the distance from the top increases. However, the experiments proved that the boundary layer influences the height at which the disruption starts. In fact, in the three boundary layers of the experiments it always starts at different levels. This will be better addressed in Chapter 6, once the CRIACIV results have been introduced. But it is now anticipated that: [a)] in the shear flow in WiSt the disruption is

observed in the pressures at 650 mm (Figure 6.9); [b)] in the uniform flow in WiSt it is observed at 450 mm (Figure 6.13); [c)] in the shear flow in CRIACIV it is observed already at 750 mm (Figure 6.9 and Figure 6.12). However, a direct relationship between this height and a certain behaviour of a boundary layer property (such as I_u, L_{ux}, L_{uz} or σ_u) has not been detected.

5.3.4 Removal of experimental (unintentional) disturbances

The peculiarity of the observed phenomenon and the lack of a direct comparison with literature arose many questions and several doubts. Therefore, during the campaign some tests were repeated in order to verify that some experimental conditions should not have appreciably influenced the occurrence of the phenomenon.

For example, since separation bubbles develop in the wake of the cylinder, it was hypothesized that the ribs in the wake might have had a disturbing effect. Therefore, a few tests were repeated by removing the ribs in the separated region, which do not have any effect on the state of the flow. In the reference condition R1 the result did not change. In case of higher roughness (e.g. R3) the asymmetric condition could stabilize even better. Therefore, ribs in the wake were not responsible at all for creating the effect.

In order to allow the ribs to adhere to the model all along the cylinder without interruption, very small cuts were done in the ring beams for passage of the ribs. Although such cuts were very small, about 1 mm, they might have acted as holes in the rings. Therefore, the tests were repeated by accurately closing all these “holes” with tesa film. The result did not change significantly, but the removal of this disturbance allowed to the asymmetric flow to stabilize better. This enhanced the idea that the design of ring beams with some holes inside would have reduced the bistable effect on the structure. In fact, the asymmetry and the inversion in different compartments create pressure differences above and below the rings. The rings prevent the vertical flow along the tower surface and enhance the interaction between compartments due to gradients of pressure. Some holes inside the rings would reduce the pressure gradients. However, this mitigation proposal has not been extensively tested and validated. The experiments available before closing the cuts in the rings did not show a disappearance of the bistable flow, just a slight disturbance (i.e. more frequent jumps).

5.3.5 The effect of the efflux

The efflux suppresses the bistable phenomenon, even with 10 rings. It is easily seen in the histograms of the lift coefficients, which are approximately symmetric and centered in zero in presence of efflux (Figure 5.19, right column).

5.3.6 The effect of number and size of rings

The number and the size of the rings play a key role. So far, the reference condition with ten big rings at a distance of 10 cm in the wind tunnel scale (100 m in full-scale if λ_L = 1:1000) has been considered. This is just one design condition, and the bistable flow depends strongly on the distribution of rings and to some extent on the size of the rings. Therefore, once the bistable phenomena were ascertained in the previously described sensitivity analysis (influence of Re, influence of surface roughness, removal of disturbances), different design cases were studied. The main results (in the no-efflux condition) are presented here and a physical explanation will be proposed in section 5.4. Then, a conclusion and a proposed recommendation will be explained in section 5.6. Figure 5.20 plots the histograms of the lift coefficients in two situations:

1) 10 small rings (KR1) on the left column;
2) 5 big rings (SR5) on the right column.

On the left column, as well as in Figure 5.19, the distance between rings is 10 cm, i.e. 2/3 of the diameter; on the left column it is 4/3 of the diameter (20 cm). A first conclusion which can be drawn from the graphs is that the flow is bistable only in case of 10 big rings and no efflux (Figure 5.19, left column). In other words, the flow is able to undergo a jump, i.e. the bubble is able to pass on the other side of the cylinder, only if the rings are sufficiently big. As it was shown in Figure 5.11, a bigger bubble develops shortly before a jump, accompanied by a stronger deviation of the stagnation angle. This bubble is the result of 3D secondary vortices in the wake due to the flow over the tip which enters the wake. The spanwise inversion is a sort of cascade effect from the highest compartment. The trigger occurs randomly in time, according to the random nature of the flow. Apparently, smaller rings do not offer enough horizontal excrescence so that sufficiently big bubbles can develop. As long as the bubbles are small they produce asymmetric flow (because they are on one side only), but they do not pass on the other side. The size of the separation bubbles, related to the size of the rings should then explain the bistability of the flow.

However, in view of the design, the bi-stability (i.e. the jump) might not be the leading feature, because it is rapid in the wind tunnel but slower in full-scale (λ_T = 488, section 4.1.2). Instead, additional stresses in the shell may arise from the stable asymmetric condition. This is still present even with 10 small rings. Therefore, more than the size of rings, it is the distribution of rings which influences the design. In any case, if the rings are small, the asymmetry is limited to a smaller range (only two compartments in Figure 5.20a). When the distance between rings is large, e.g. 20 cm on the 1 m model

(whose diameter is 15 cm), both the bi-stability and the asymmetry vanish (Figure 5.20 right column). Increasing the distance between rings is then a safe mitigation strategy.

SR1-EF0: 10 big rings - without efflux (C_L) *SR1-EF1: 10 big rings - with efflux (C_L)*

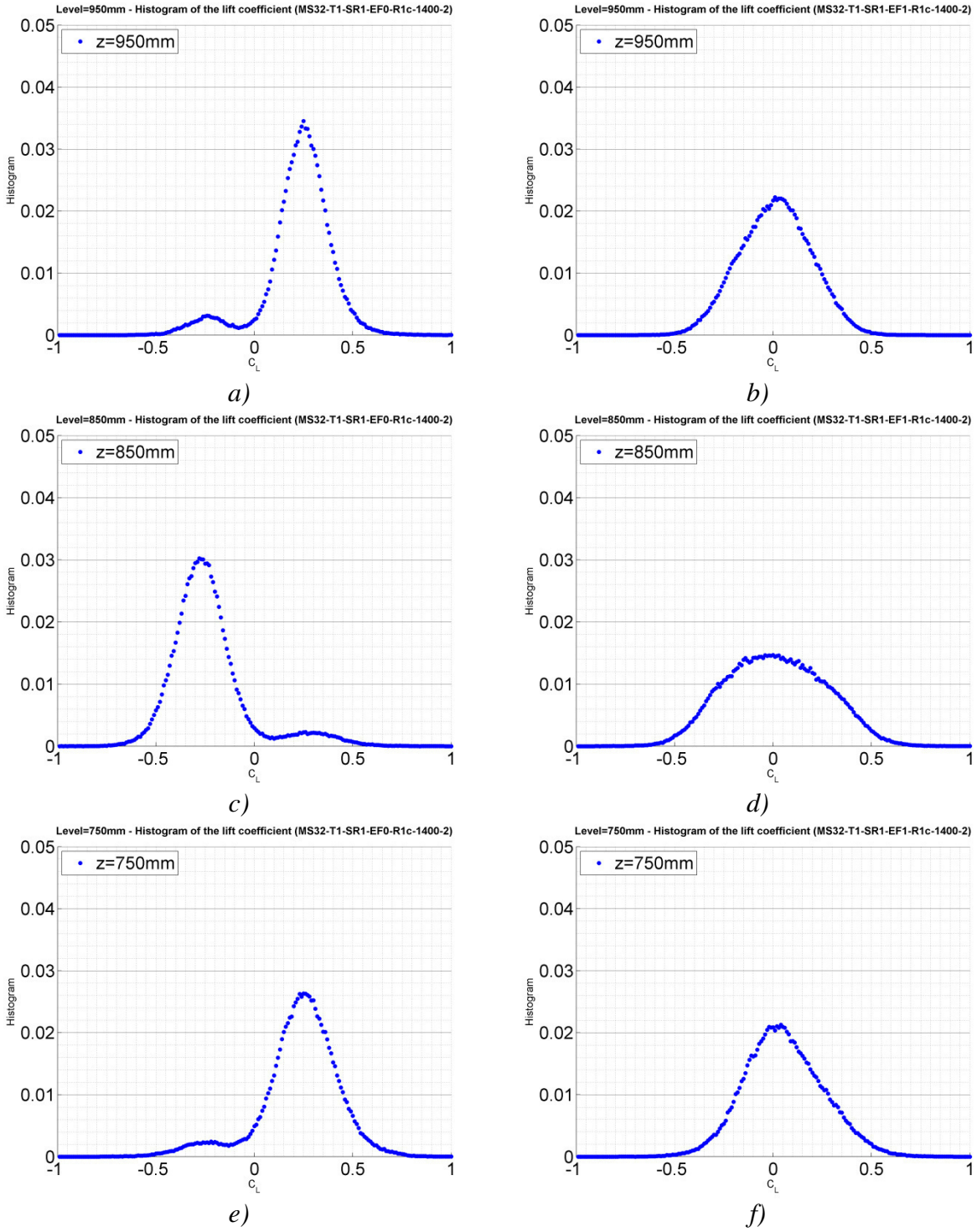

Figure 5.19 Effect of efflux on the bistable flow with 10 rings, histograms of C_L: a) level 950 mm (EF0); b) level 950 mm (EF1); c) level 850 mm (EF0); d) level 850 mm (EF1); e) level 750 mm (EF0); f) level 750 mm (EF1); (WiSt, T1-SR1-R1-EF0/EF1)

KR1-EF0: 10 small rings - without efflux (C_L) *SR5-EF0: 5 big rings - without efflux (C_L)*

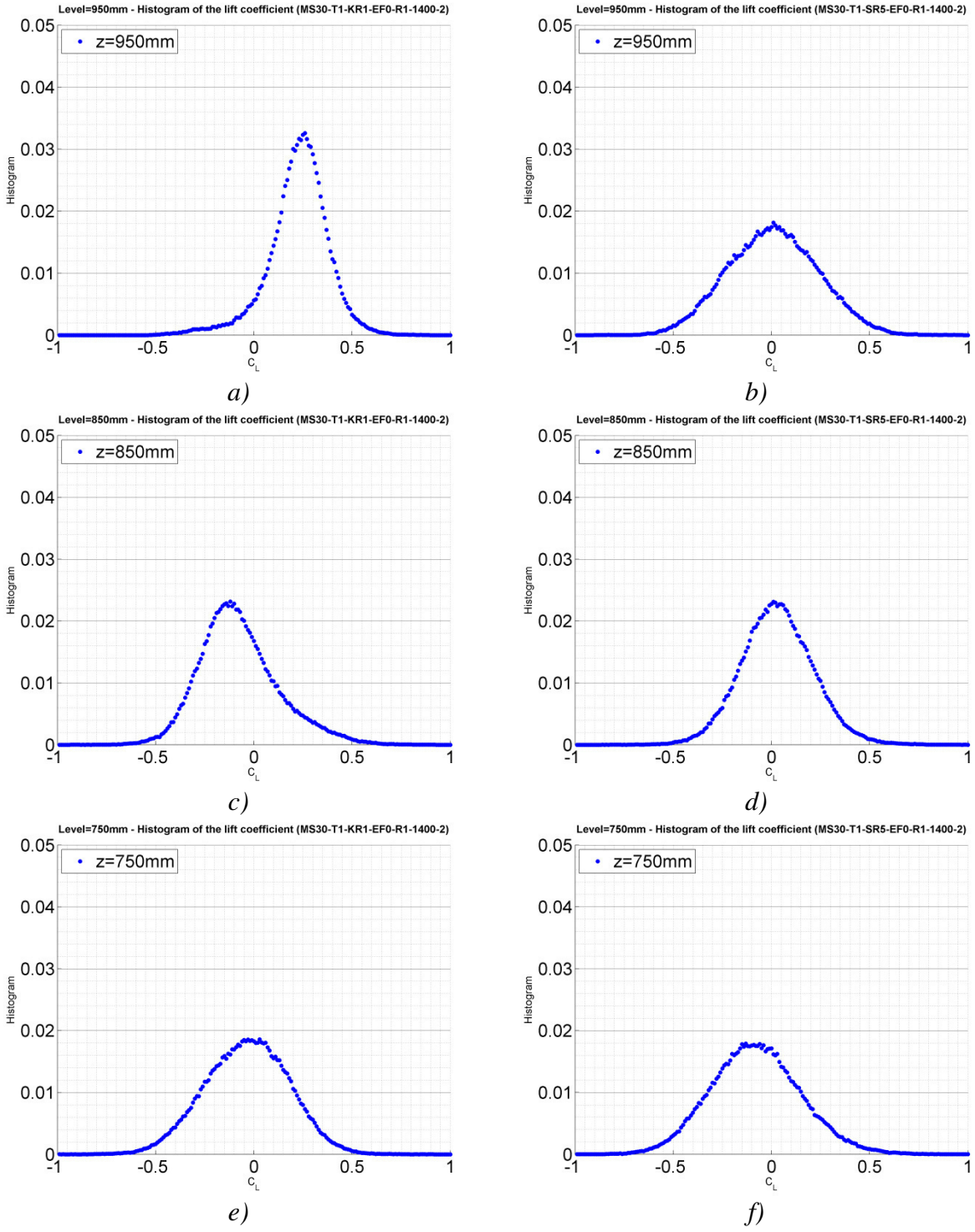

Figure 5.20 Effect of size and number of rings on the bistable asymmetric flow, histograms of C_L: a) level 950 mm (KR1); b) level 950 mm (SR5); c) level 850 mm (KR1); d) level 850 mm (SR5); e) level 750 mm (KR1); f) level 750 mm (SR5); (WiSt, T1-KR1/SR5-R1-EF0)

5.4 A physical interpretation

The key points of the cross-wind phenomenon described so far are first remembered in a brief summary.
Pressure measurements on 1 m circular cylinder with 10 rings of 7 mm in width at spacing of 100 mm (scale 1:1000 to the prototype) have shown:

1. two steady asymmetric states (namely “state 1” and “state 2”);
2. a bi-stability of the flow, i.e. a change of state in time;
3. a spanwise inversion, i.e. a change of state in space.

It was not found, at increasing Re, any tendency for this phenomenon to disappear. Instead, the phenomenon is cancelled out by the efflux and the effect is mitigated by using fewer and/or smaller rings.
The phenomenon is more evident in the upper part of the tower, this would support the thesis that it is a 3D effect, related to the free-end. The occurrence of the phenomenon does not depend significantly on the atmospheric boundary layer. The characteristics of the atmospheric boundary layer are not governing parameters, they only influence the development – or the disruption – of the phenomenon along the height. The spanwise inversion may be interpreted as a cascade effect in the neighbouring compartments, starting from the highest one. The change of state in time, i.e. the jump, appears randomly: no periodicity has been found. This random nature of the bi-stability reflects the random nature of turbulent flow. Relying on the wind tunnel measurements, it is not straightforward to state that a symmetric state can be obtained if an infinitely long period is considered. In fact, the asymmetric conditions, once formed, tend to establish. Each state is intrinsically stable. The change of state must then receive some stronger input from the flow in order to initiate and take place. It is not astonishing, therefore, that sometimes this input is not found in the time window of a measurement. In any case, asymmetric states generally persist so long that the design of the structure should necessarily include the asymmetric interval, even though the structure is symmetric.
Secondary vortices like separation bubbles develop in the wake on one side only of the cylinder, that is called in this work “bubble side”. A key role, from the fluid-dynamic point of view, is the near-wake structure. In fact, the structural design is not directly governed by wake fluctuations, but the development of a certain wake structure and a vortex street are responsible for cross-wind loads and body-induced fluctuations in the attached boundary layer before separation.

An in-depth examination of the cross-wind phenomenon introduced in section 5.2 has led to the physical interpretation proposed in the following. The focus is not in the jump between two states, rather on the asymmetric steady condition within each state.
Von Karman vortex separation produces an oscillation of the separation point. Instantaneously, the pressure distribution is not symmetric, but the lateral suction increases on the side of the cylinder where the vortex is growing, before being shed. However, the phenomenon described in section 5.2 is not dealing with an instantaneous asymmetry of pressures, which produces an oscillating cross-wind force. This would be the well-known phenomenon of vortex separation. Instead, section 5.2 describes a steady asymmetric state, which produces a mean lift. This is a first fundamental characteristic. Therefore, the asymmetry must be sought at first in the averaged position of the separation point in the mean pressure distribution. Separation angles are identified at z/H = 0.95 in Figure 5.21, referring to the state 1.

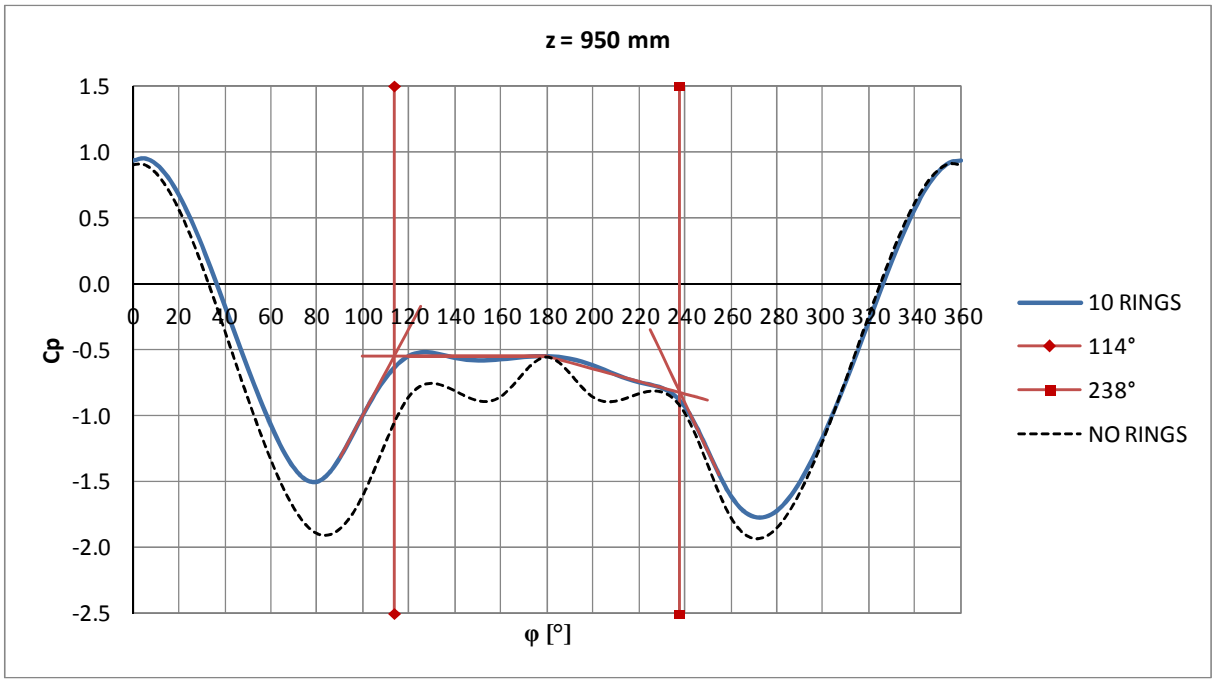

Figure 5.21 Mean pressure distribution and separation angles (WiSt, T1-SR1/SR0-R1-EF0)

Figure 5.21 describes the horizontal distribution and the strong asymmetry at a certain cross-section (z = 950 mm), but it cannot say anything about the three-dimensionality of the effect within the compartment and between different compartments. This issue is better addressed – in a first stage – by the cross-correlation coefficients; then they will be split up in the frequency domain. Since the phenomenon is a sort of cascade effect from the highest compartment (i.e. compartment number 10), the cross-correlations within this compartment and between it and the neighbouring one are investigated, both far from the rings and close to them. One state is considered alone.

Figure 5.22 shows the circumferential cross-correlations within compartment number 10, i.e. between levels z_1 = 950 mm and z_2 = 910 mm. The continuous line refers to the case with 10 rings (SR1), while the dashed line refers to the case without rings (SR0). At stagnation and for a certain region downstream the presence of rings does not modify the cross-correlations within the compartment: the ring beam is like not-existing. Then, at a certain angle, the cross-correlations SR1 drop down significantly. The asymmetry of the mean pressure distribution is also confirmed in the cross-correlations, because such a drop starts earlier on one side of the cylinder (0°-180° in this case). By looking at Figure 5.21, it can be seen that the drop starts earlier on the normal side. The earlier drop in the correlations likely reflects an anticipated separation of the boundary layer on the normal side of the cylinder, with respect to SR0, where separation is normally at large angles due to the tip effect. Since the cross-correlation is between two levels (z_1 = 950 mm, z_2 = 850 mm), the earlier separation may occur either at the level z_1, or at the level z_2, or on both levels.

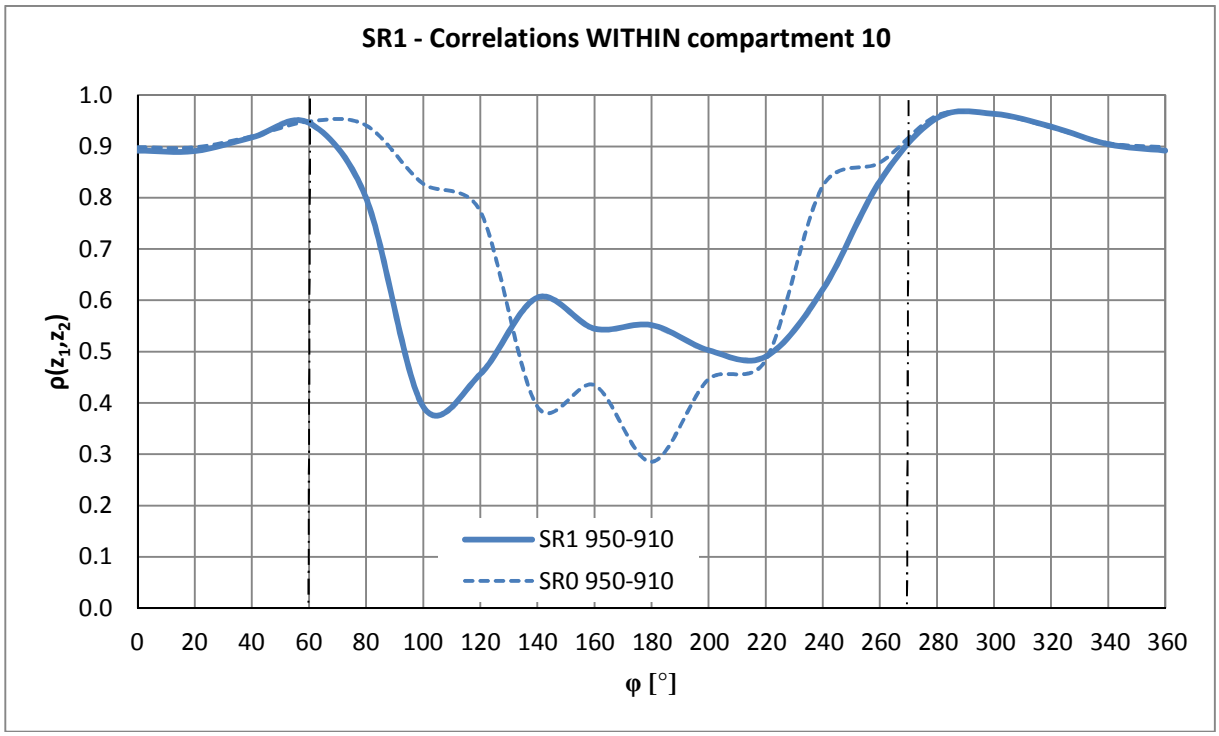

Figure 5.22 Cross-correlations of C_p between two levels
10 rings (continuous line SR1), without rings (dashed line SR0)
z_1 = 950 mm, z_2 = 910 mm (WiSt, T1-SR1/SR0-R1-EF0)

Let us consider the reference height z_1 = 950 mm, as before. Figure 5.22 described the cross-correlations of this level within the compartment. Now, the cross-correlations with the neighbouring compartment are added (Figure 5.23 and Figure 5.24). In particular, Figure 5.23 shows the cross-correlations of z_1 = 950 mm with a level close

to the ring n.9 (below it, z_2 = 890 mm) and Figure 5.24 shows the cross-correlations with a level in the middle of the compartment below (z_2 = 850 mm). It must be remembered, from Figure 5.22, that ρ(950,910) drops early on one side at about 60° due to the effect of the ring. It is now remarkable to see that such an earlier drop on the same side of the cylinder, i.e. at 60°, does not appear neither in Figure 5.23 nor in Figure 5.24. In fact, ρ(950,890) and ρ(950,850) are not affected by the rings until about 90°-100°. Instead, perfectly consistent with the inversed mirrored condition previously described in terms of $C_{p,m}$ and $C_{p,\sigma}$, an earlier drop at 300° (i.e. -60°) occurs in ρ(950,890). Even more remarkable, is that the correlation between middle levels in different compartments (950 and 850 mm) does not perceive the earlier drop (Figure 5.24). This suggests that the effect of the ring is an earlier separation that develops within the compartment on one side only of the cylinder, as we move closer to the ring. The cross-correlations between middle levels remain unaffected much longer downstream.

In Figure 5.22, the movement towards the ring is from above (because $z_1 > z_2$) and the earlier drop is at 60°. Figure 5.25 (ρ(850,890)) is like Figure 5.22 – i.e. it shows the cross-correlations within the compartment – but in the compartment below. The reference level is z_1 = 850 mm and the movement towards the ring is from below (z_1 = 850 mm < z_2 = 890 mm). The cross-correlations confirm not only the asymmetry of the pressures, but also the inversion between different compartments, because the earlier drop in the cross-correlations ρ(850,890) occurs mirrored with respect to Figure 5.22, i.e. at 300°.

Therefore, the earlier drop of the correlation coefficient on one side only of the cylinder (normal side) and close to the ring (either above or below it) is explained by an earlier separation of the boundary layer at the ring (earlier than in absence of rings). On the other side of the cylinder, as well as in the neighbouring compartment on the same side, instead, the flow remains longer attached (separation is delayed). That is the bubble side. This movement of the mean separation line induced by the rings is confirmed by the mean pressure distributions calculated during only one state: the separation line is not at a symmetric position on the two sides of the cylinder (thus the steady asymmetry results, as shown in Figure 5.26 and Figure 5.27) and presents a discontinuity at the ring. In other words, the wake is not aligned in the rear of the cylinder.

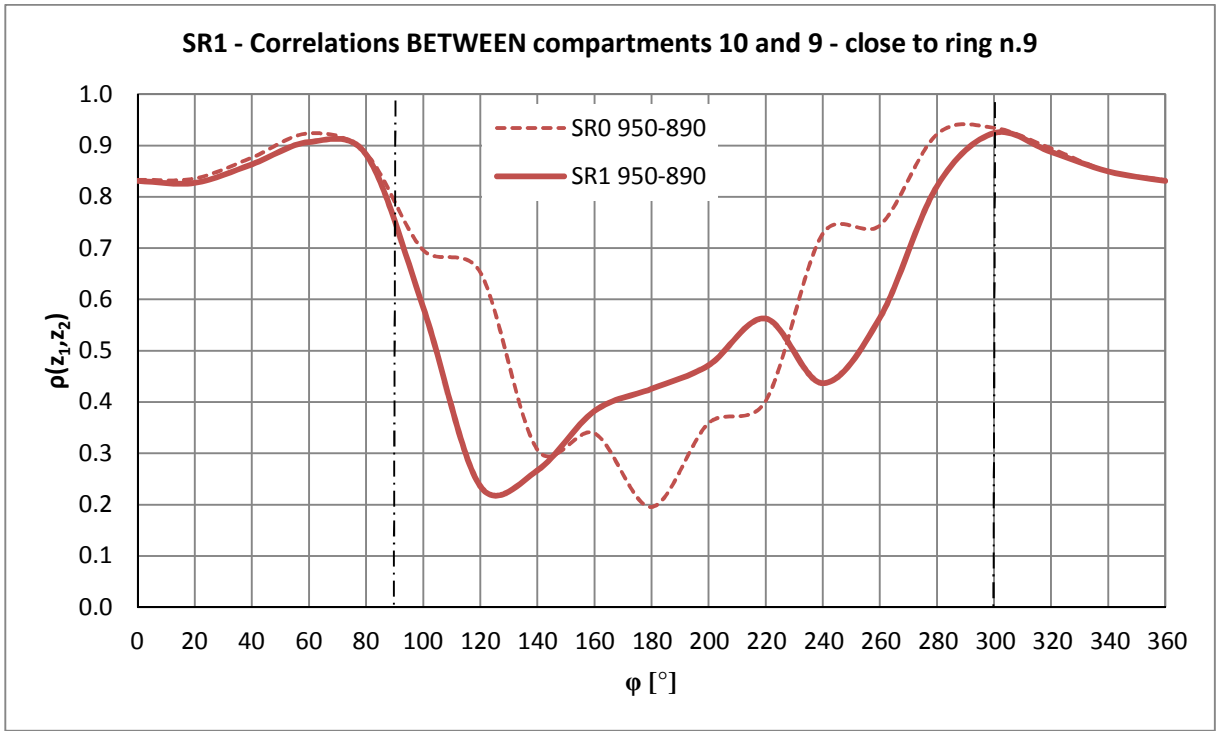

Figure 5.23 Cross-correlations of C_p between two levels
10 rings (continuos line SR1), without rings (dashed line SR0)
z_1 = 950 mm, z_2 = 890 mm (WiSt, T1-SR1/SR0-R1-EF0)

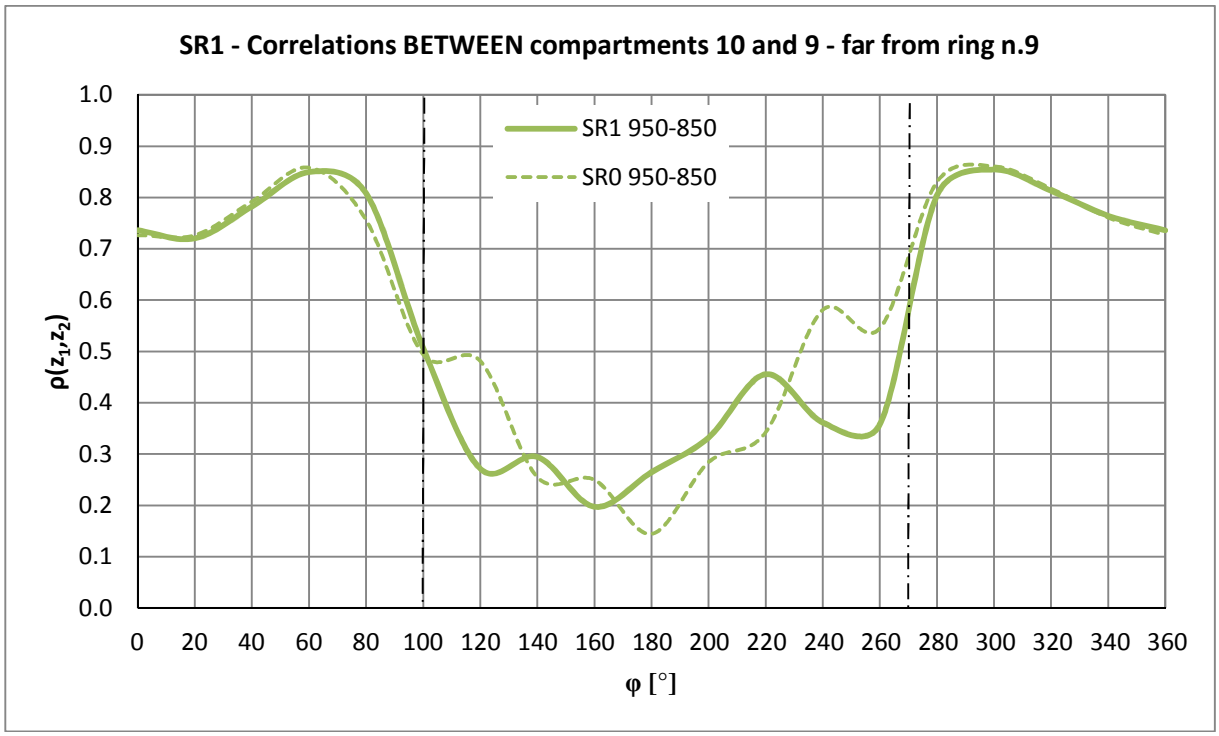

Figure 5.24 Cross-correlations of C_p between two levels
10 rings (continuos line SR1), without rings (dashed line SR0):
z_1 = 950 mm, z_2 = 850 mm (WiSt, T1-SR1/SR0-R1-EF0)

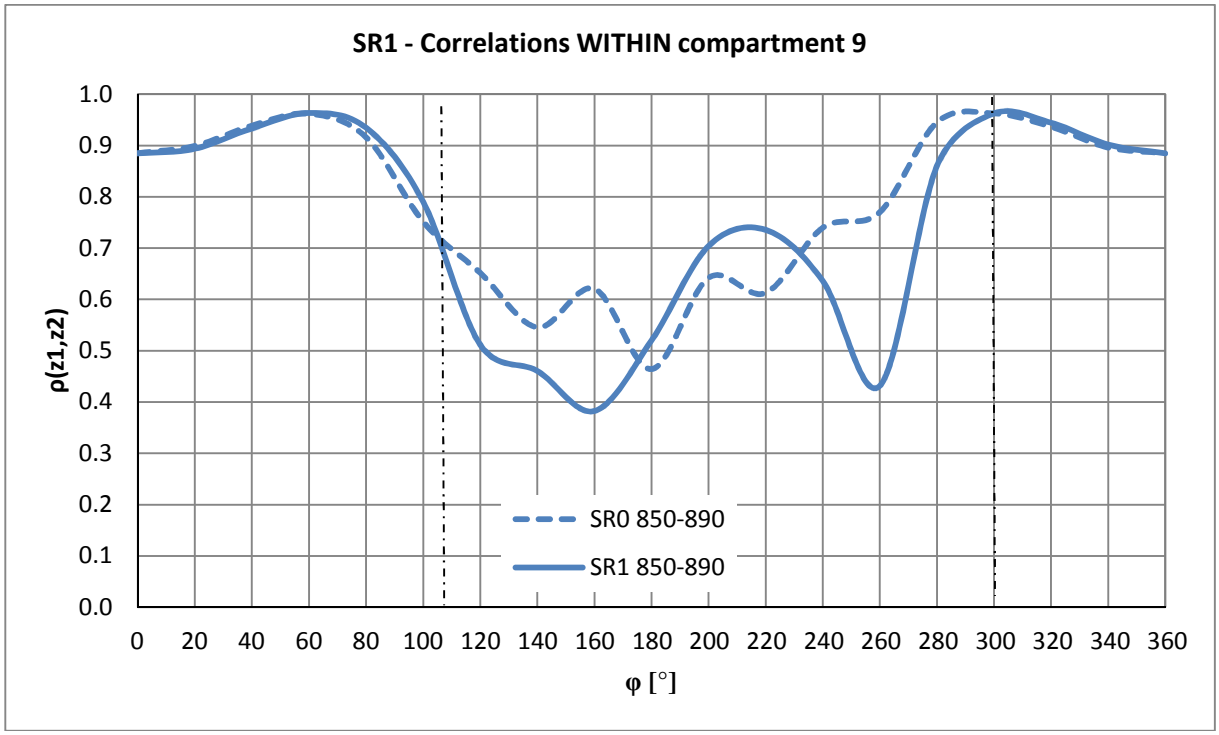

Figure 5.25 Cross-correlations of C_p between two levels 10 rings (continuos line), without rings (dashed line): z_1 = 850 mm, z_2 = 890 mm (WiSt, T1-SR1/SR0-R1-EF0)

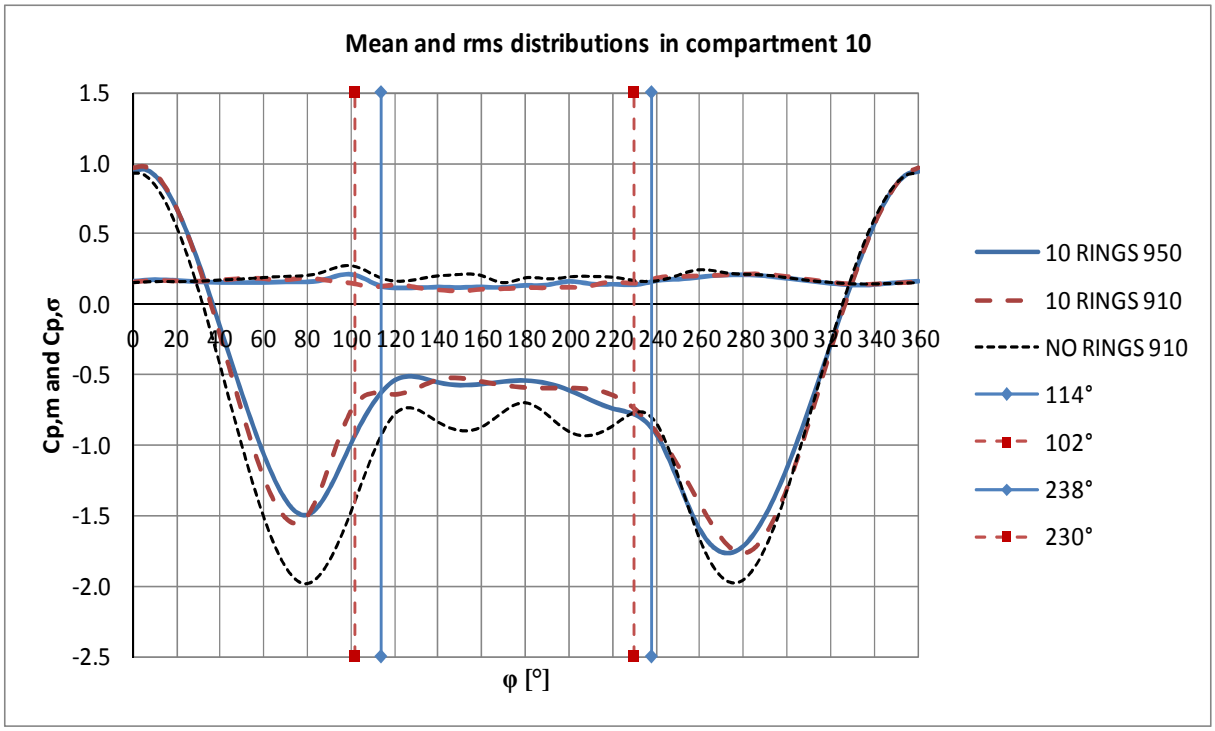

Figure 5.26 Angles of separation in the compartment n.10 (WiSt, T1-SR1/SR0-R1-EF0)

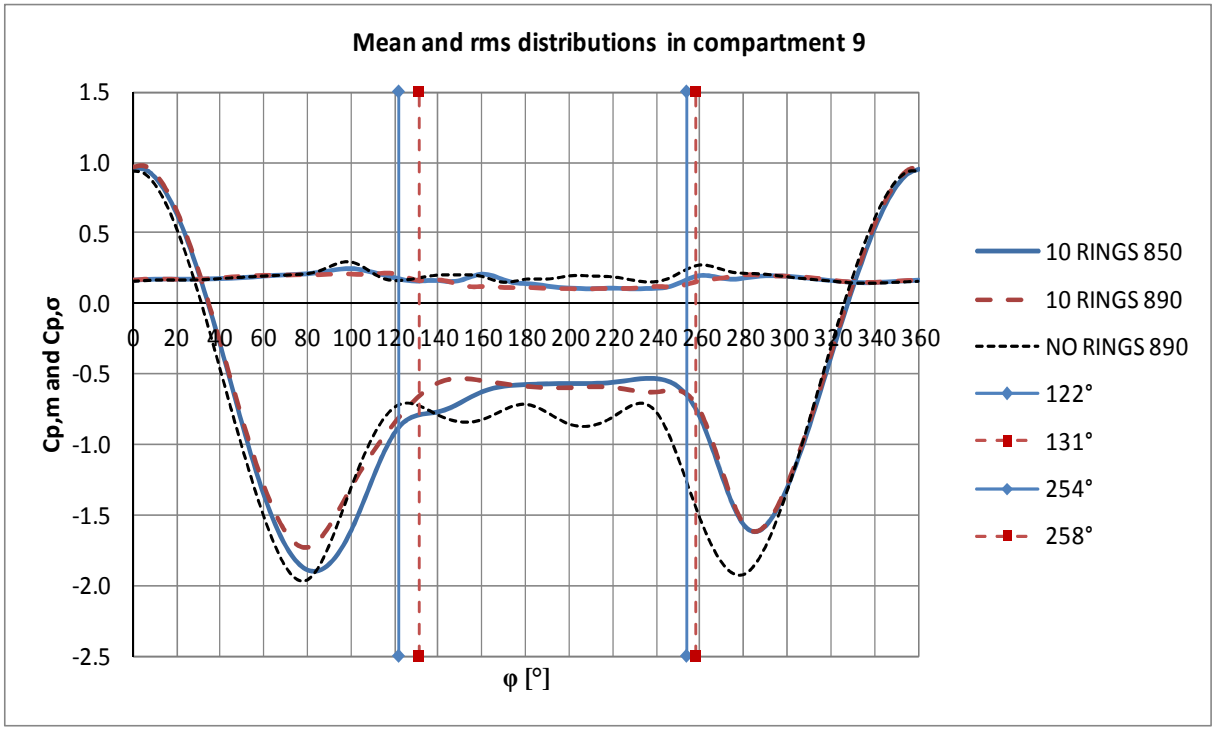

Figure 5.27 Angles of separation in the compartment n.9 (WiSt, T1-SR1/SR0-R1-EF0)

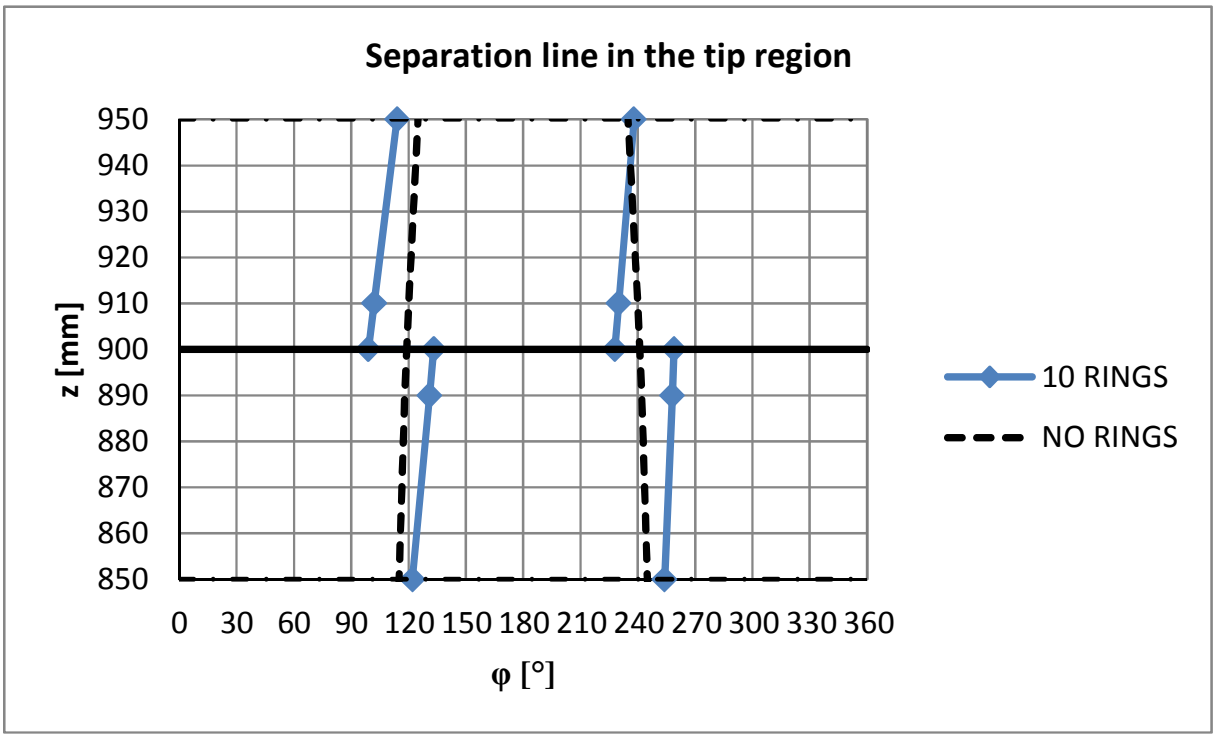

Figure 5.28 Discontinuity of the mean separation line within one state (WiSt, T1-SR1/SR0-R1-EF0)

A jump between two states produces an inversion of the position of the separation line around the circumference. Then, around the circumference, there is an appreciable movement of the mean position of separation, which can be identified in the pressure measurements. For example at the level 890 mm, the separation point oscillates around two different mean positions, which alternate in time: one is before 120° and one is after that. Therefore, the time history recorded at φ = 120° shows two different states of the flow (Figure 5.29): the pressure tap lies once in the attached boundary layer before separation (higher rms) and once in the wake (lower rms).

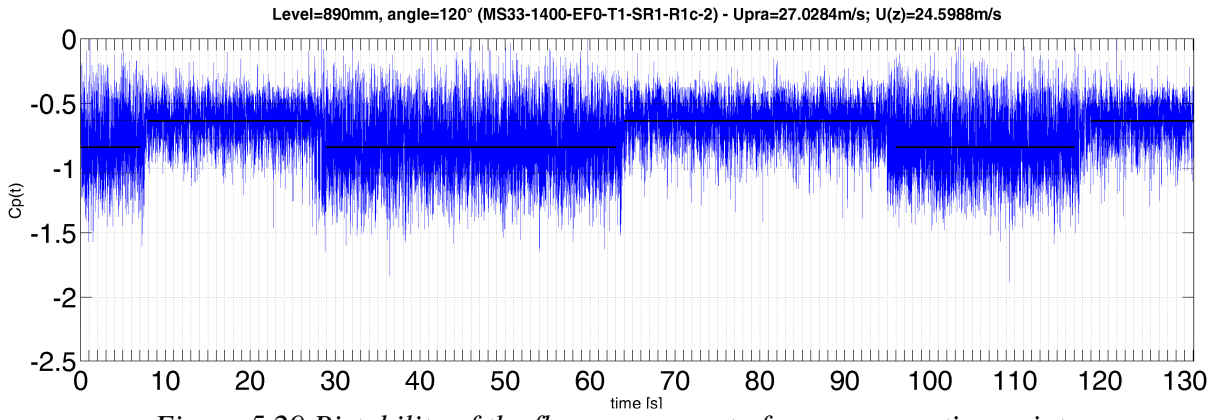

Figure 5.29 Bistability of the flow: movement of mean separation point (WiSt, T1-SR1-R1-EF0)

Figure 5.22 (referring to compartment n. 10) showed an anticipated drop of the cross-correlation coefficients on the side 0°-180° in case of ten rings. The same happened in the compartment below on the side 180°-360° (Figure 5.25). It is now interesting to split up the cross-correlation coefficients between two levels at a certain angle in the frequency domain (Co-spectrum(z_1,φ_1; z_2,φ_1)/$\sigma_1\sigma_2$), in order to indentify the missing contributions with respect to the case without rings. The angle 100° and 260° are chosen as reference in both compartments 10 and 9. In particular, the angle 100° lies on the normal side in compartment 10 and on the bubble side in compartment 9. The opposite holds for the angle 260°. Figure 5.22 and Figure 5.25 show that ρ(950,910) at 260° and ρ(850,890) at 100° (bubble sides) are basically the same both in presence and in absence of rings (SR1 and SR0). It is then surprising that the difference in case of rings is on the so-called normal side. The missing contribution in SR1 can be identified in the frequency domain. It results to be a typical 3D effect of circular cylinders with a free-end. It is a proof that the rings interact, somehow, with the three dimensional flow. In fact, Figure 5.30 a), d) shows that the missing contribution in the co-spectra of C_p on the normal sides (0°-180° in compartment 10 and 180°-360° in

compartment 9) are not in the frequency range of Karman vortex shedding (nD/U ≈ 0.2), but at lower frequencies.

In order to understand the phenomenon created by the rings, it is now important to go one step back and investigate deeper the flow around the free-end, even in absence of rings. So far, the effect of the rings has been described as an asymmetric pressure distribution, associated to a fragmented separation line and a misaligned wake of the cylinder. The study of the cross-correlations within the same compartment and in different compartments has suggested that an earlier and a delayed separation develops at the rings. The phenomenon evolves within the compartment as one moves towards the ring; the cross-correlations at middle levels between rings are not affected much longer downstream. The frequency split-up of the cross-correlations at about 100° between different levels allowed to identify the range of frequencies where, in presence of rings, the phenomenon acts. It is not the range of Karman vortex shedding ($S_t \approx 0.2$). Rather, it is a lower range, that results to be – by literature documentation – the frequency range of TAV, tip-associated-vortices (Kitagawa et al., 2001).
Tip-associated-vortices, described in Chapter 3, should not be confused with the longitudinal trailing vortices at the tip of the cylinder, which are created by the interaction between the upwards flow at the flanges and the downwards flow over the tip. The TAV are bigger Karman vortices, at a frequency around one third of the usual Karman frequency at intermediate levels. They are responsible for the variation of the Strouhal number in the tip region which is produced, according to Farivar (1981), by the entrainment in the wake and elongation of the eddy formation region. The tests performed by Kitagawa et al. (2001) constitute, so far, one of the deepest investigations of TAV. Those tests are performed in uniform flow on a H/D = 26 circular cylinder. Therefore, it is not surprising that the TAV are confined at high-levels and do not interact with the Karman vortex shedding at middle height (Figure 3.34c). A different situation and a stronger interaction should be expected on a H/D = 7 circular cylinder. In fact, in our experiments, double-peak spectra – low frequency peak due to TAV and Strouhal peak due to Karman vortex shedding – describe the cross-wind fluctuations at the high levels in SR0. As it will be shown in Chapter 6 by comparison with CRIACIV, the boundary layer influences the either stronger or weaker interaction between the two peaks at different levels. In any case, there is general agreement on the shedding frequency of TAV, about nD/U = 0.07, as confirmed by Kitagawa et al. (2001) and Park&Lee (2000). The results of the present work in SR0 are a further confirmation.

Compartment n. 10 (900-1000 mm):

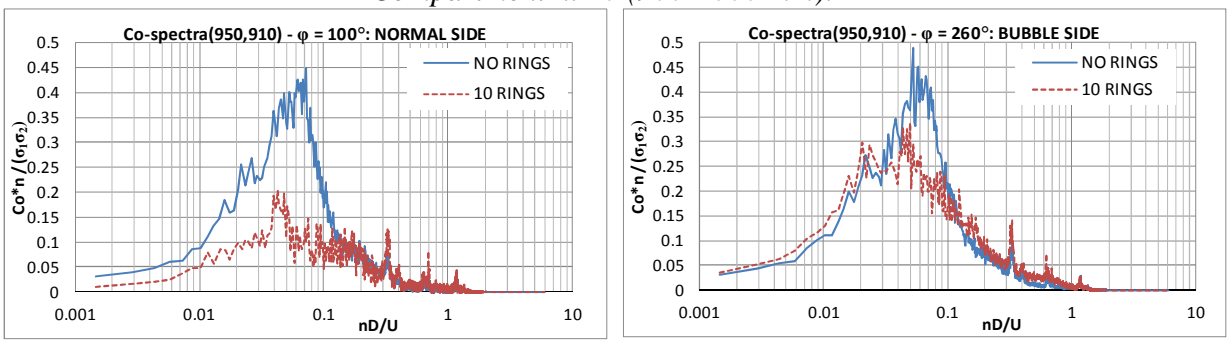

a) *b)*

Compartment n. 9 (800-900 mm):

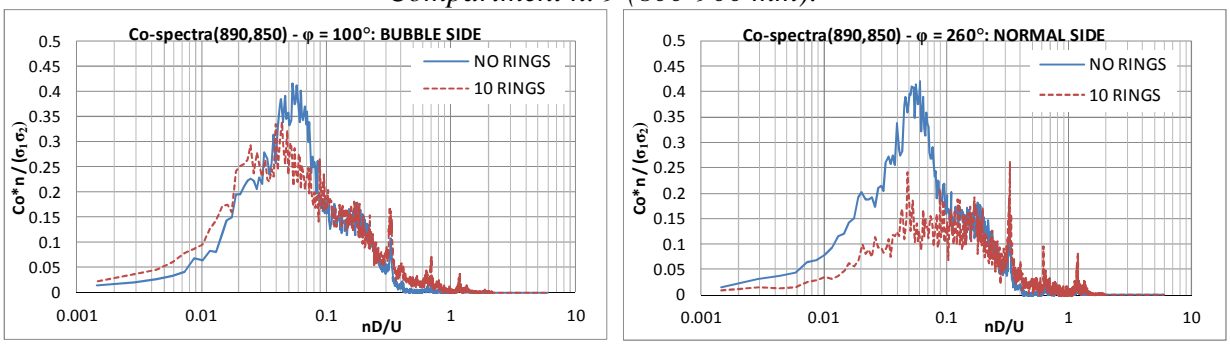

c) *d)*

Figure 5.30 Asymmetry of the of the flow in the frequency domain:
blue line: no rings; red line: 10 rings;
a) Co(950,910) at 100°; b) Co(950,910) at 260°;
c) Co(850,890) at 100°; d) Co(950,890) at 260°;
x-axis: nD/U_{1000}; y-axis = $Co_{Cp}(z_1,z_2)*n/(\sigma_1\sigma_2)$;
(WiSt, T1-SR0/SR1-R1-EF0)

Figure 5.31 shows the strong interaction in absence of spanwise rings between the low-frequency peak at nD/U = 0.062 and $S_t = 0.2$.

The TAV predominate at z/H = 0.95, where the Karman vortex shedding is weak (but not completely absent).

At z/H = 0.85 there is a strong interaction between the two peaks and then the low-frequency peak disappears at $z/H \leq 0.75$. Only a skewness of the spectra remains.

It is also observed (not shown) that in presence of efflux the low-frequency peak disappears. In Chapter 7 the effect of the low-frequency peak on the response will be investigated. It essentially gives a contribution in the quasi-static oscillation, on which Karman resonance is superimposed.

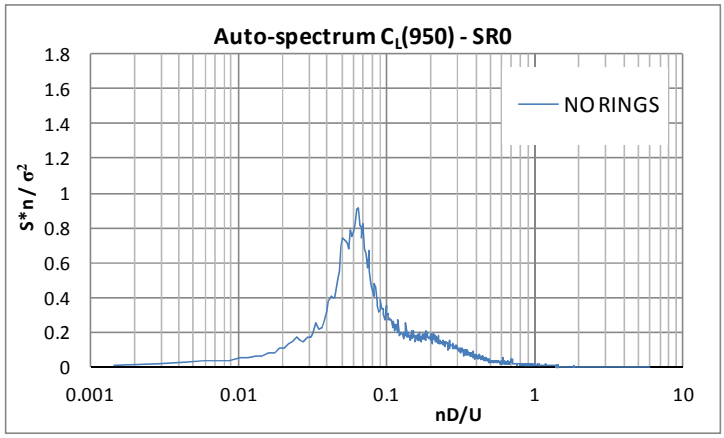

a) z = 950 m

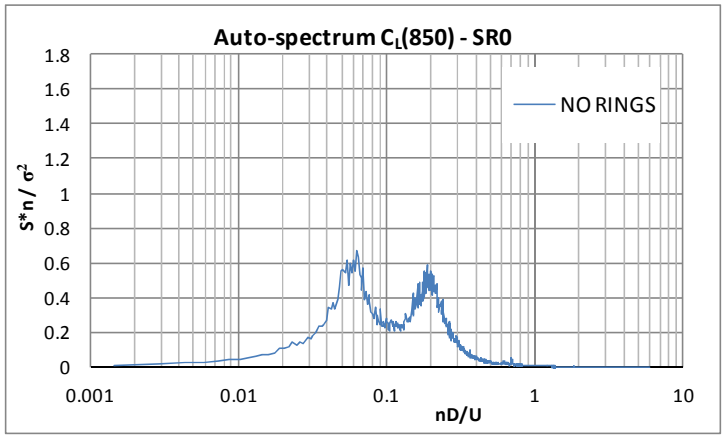

b) z = 850 m

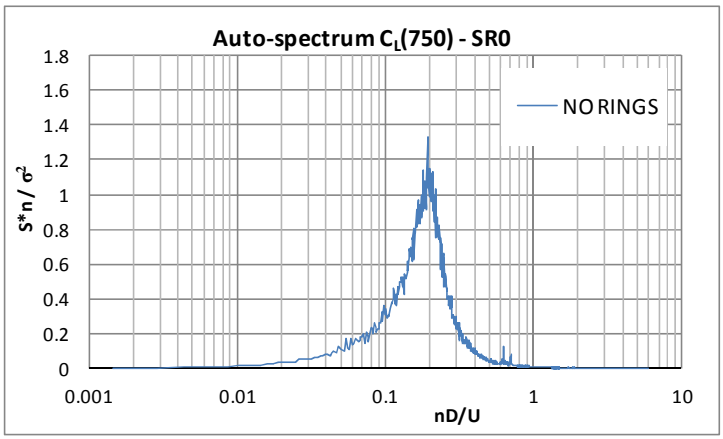

c) z = 750 m

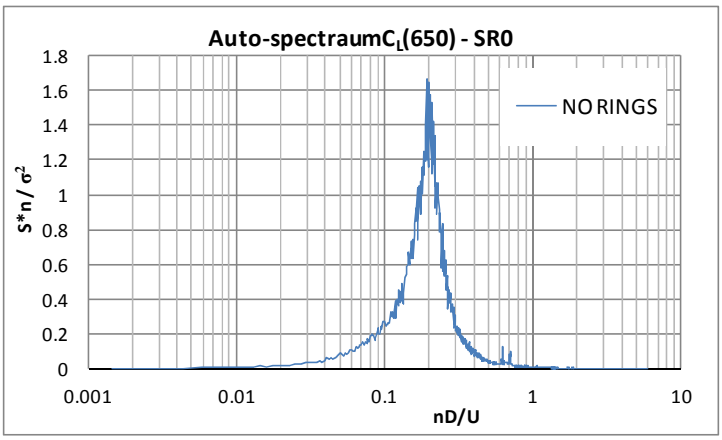

d) z = 650 m

Figure 5.31 Lift spectra along the height without rings (WiSt, T1-SR0-R1-EF0)

In this section, it is interesting to analyze the effect of the rings on the TAV. It is interesting to see in Figure 5.32 that the spectra of lift coefficients in the tip region are not double-peak spectra (as they are in SR0), but they present only one peak at Strouhal number 0.2 (von Karman vortex shedding). Actually, it was for this reason, that the spectral analysis in case of ten rings alone could not say so much, before being compared with the corresponding case without rings. The single-peak lift spectra in SR1 appeared to be perfectly reasonable at first sight. Only the comparison with the results of the circular cylinder without rings highlighted the disappearance of tip-associated-vortices.

In terms of pressures, Figure 5.30 has suggested that the low frequency peak due to tip associated vortices is fragmented on the normal side of the cylinder at each level, while such bigger vortices still remain on the bubble side. These big vortices associated to low frequency contributions, which remain on one side only of the cylinder, are responsible for the delayed separation on the bubble side. This explains also the asymmetry. Moreover, since low frequency tip-associated vortices are fragmented on one side of the cylinder in case of ten rings, they do not produce lift fluctuations: the low-frequency peak in the lift disappears.

Compartment n. 10 (900-1000 mm):

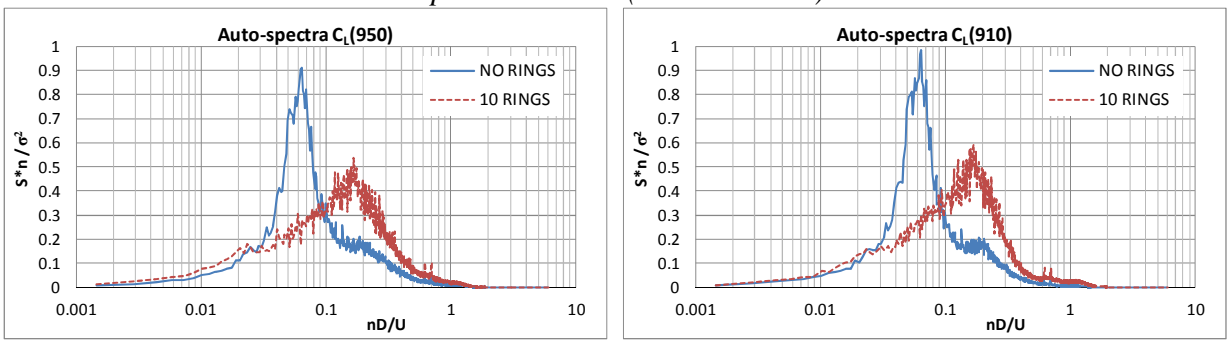

a) *b)*

Compartment n. 9 (800-900 mm):

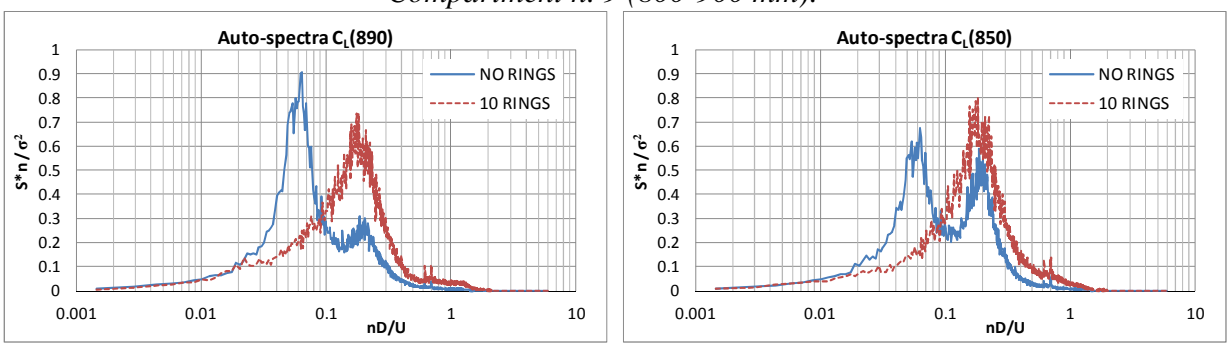

c) *d)*

*Figure 5.32 a-d) Lift spectra at 950-910-890-850 mm. $S_{CL}(z_1)$*n/σ) vs nD/U_{1000}; (WiSt, T1-SR0/SR1-R1-EF0)*

Kitagawa et al. (1999) placed a circular disk (not a ring) on the top of a circular cylinder of finite length and observed the disappearance of tip vortices. The disk had a diameter of 1.6 times the tower diameter. A smaller disk (with a diameter 20% larger than the tower diameter) was not able to suppress the tip vortices, it just reduced their strength. Kitagawa concluded correctly that the tip vortices were produced by the free-end and therefore some modification of the free-end conditions would have altered them. One may then think that the top ring on the solar tower could have, alone, the same effect as the disk placed by Kitagawa, although the diameter of the ring is only 10% larger than the tower diameter, comparatively smaller than what Kitagawa observed. Due to the small dimensions of the ring, such a strong effect would be surprising. In fact, by adding the results of the tests with the five ringed cylinder, a new explanation can be supposed.

Figure 5.33 shows the vertical cross-correlations of lift forces between different compartments. The reference level is 950 mm. A similar picture (Figure 6.15) will also be shown in Chapter 6 as further proof. Figure 5.33 shows that the lift cross-correlations in case of five rings follow the same bahaviour as in SR0 (no rings). The co-spectra divided by the product of the standard deviations, i.e. the split up over frequencies of the cross-correlation coefficients, prove that in case of five rings the tip vortices are not suppressed. It should also be remembered (Figure 5.20) that in case of five rings the flow is neither asymmetric nor bistable. Instead, in case of ten rings, $\rho,C_L(950,850)$ (i.e. ρ,C_L (Δz=100)) is much lower because the contribution of the tip-associated vortices is missing.

It follows that a certain distribution of rings, at a sufficiently small distance, interacts and kills the bigger vortices in the tip region. It should also be observed that in case of ten rings the distance between them is 10 cm in the scale of the wind tunnel model (i.e. 2/3 of the diameter) and in case of five rings the distance between them is 20 cm (i.e. 4/3 of the diameter). Between 10 and 20 cm, the value 15 cm lies. This is actually the tower diameter. Although so far there is not an experimental proof of it, it can be supposed that the tower diameter could be taken as reference to calibrate the distance between rings, in order not to interact with tip vortices. Even more, it could be supposed that, since the big tip vortices develop only in the tip region, the key feature is the distance between rings only in the tip region and not all along the tower. In this regard, Chapter 8 will mention, among future outlooks, the importance of doing tests where the ring beams are not equally distributed along the heihgt, but they are placed at larger distance (e.g. 4/3D) in the tip region only.

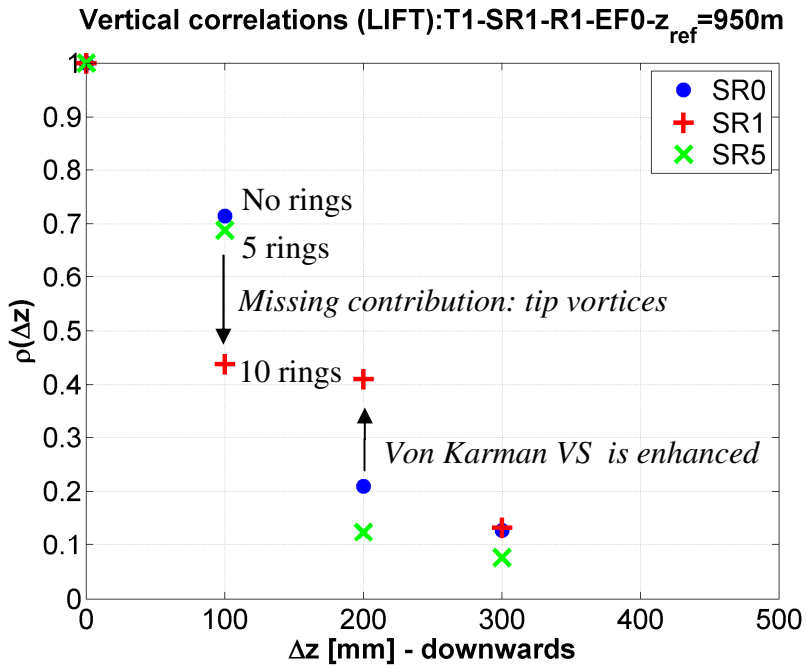

Figure 5.33 Cross-correlation coefficients of C_L without rings (blue), 10 rings (red) and 5 rings (green). z_{ref} = 950 mm (see also Figure 6.15)

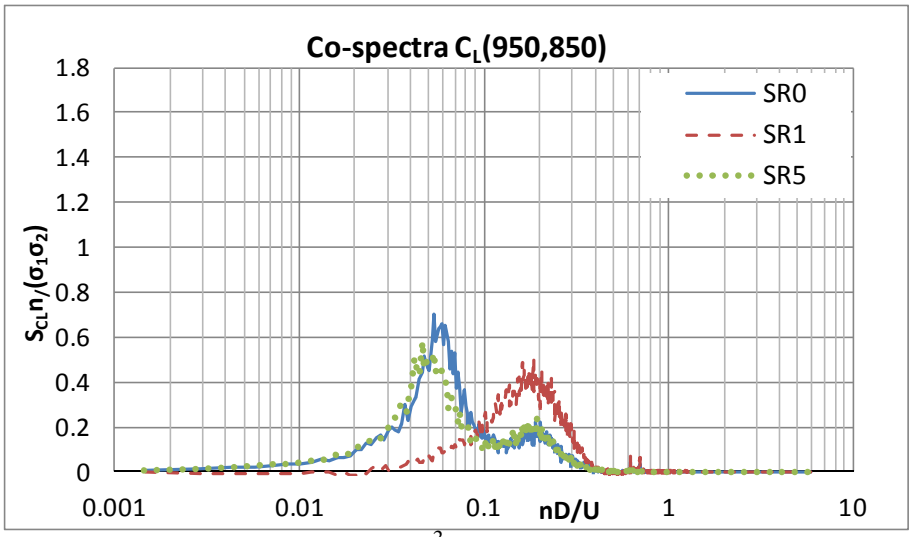

Figure 5.34 Co-spectra of C_L: $S_{CL}(z_1,z_2)*n/\sigma^2$ vs nD/U, z_1 = 950 mm, z_2 = 850 mm; (see also Figure 6.16). (WiSt, T1-SR0/SR1/SR5-R1-EF0)

A further proof that the tip vortices are disturbed by rings placed at a too small distance is given by the experiments with 10 small rings (KR1). In that case, the flow is not able to undergo jumps, but it is asymmetric (Figure 5.20). Figure 5.35 shows that ten rings, at a smaller distance than the diamter (2/3 of it, in this case) are able to suppress tip associated vortices, even if the rings are small. Figure 5.36 proves that the Karman vortex shedding ($S_t \approx 0.2$) is not significantly affected by the rings. The low-frequency contributions in the spectra of SR1-SR5-KR1 represent the oscillations produced in the time histories by the changes of state (e.g. in Figure 6.9 at 650 mm).

The spectra are evaluated separately in each interval of time, the intervals are clearly detectable for example by looking at the time histories of either lift force or pressures in the tip region (see Figure 5.3 and Figure 5.4, the selection of intervals is evident). However, as it will be better explained in Chapter 6 (Figure 6.12), the stability within each state is progressively lost at low levels and even within the same interval of time the frequency of jumps between the two states increases. However, a predominant low frequency peak cannot be identified.

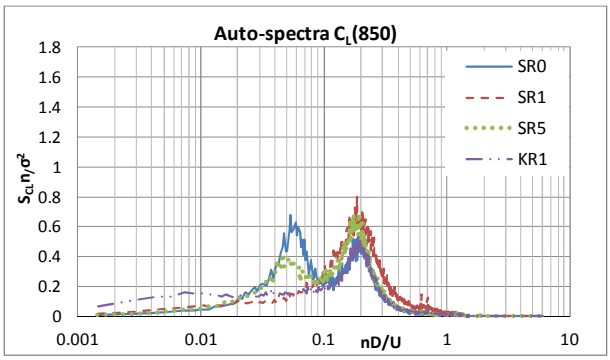

Figure 5.35 Lift spectra at 850 mm. $S_{CL}(z_1)*n/\sigma^2$ vs nD/U_{1000}; (WiSt, T1-SR0/SR1/SR5/KR1-R1-EF0)

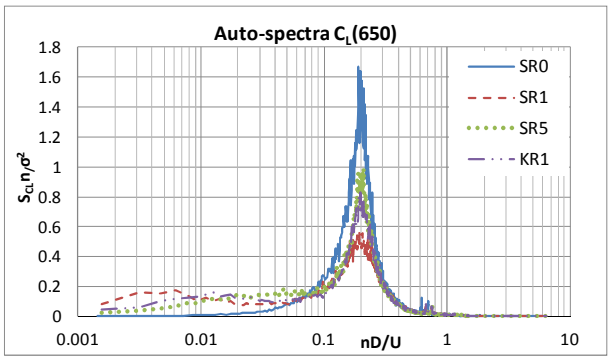

Figure 5.36 Lift spectra at 650 mm. $S_{CL}(z_1)*n/\sigma^2$ vs nD/U_{1000}; (WiSt, T1-SR0/SR1/SR5/KR1-R1-EF0)

The auto-spectra are normalized with respect to the variance, so that the area is one. The following table reports the variances, for the sake of completeness.

Table 5.1 Variances of C_L

C_L,σ^2				
	SR0	**SR1**	**SR5**	**KR1**
950	0.020	0.014	0.053	0.027
850	0.033	0.017	0.034	0.042
750	0.020	0.022	0.053	0.044
650	0.022	0.039	0.030	0.035

The TAV are a typical three dimensional effect due to the free-end: the reason for the lower frequency contribution close to the top is the entrainment of flow in the wake from above the cylinder, as previously said. The numerical simulations in Chapter 6 will clarify that the entrainment of flow in the wake results to be significantly altered by the presence of rings. This motivates not only the disappearance of tip-associated-vortices, but also the asymmetry and the spanwise inversion.

It is straightforward to wonder what it may happen if the entrainment in the wake is prevented, for example by an end-plate. In other words, what would happen in 2D

flow? Within this work, it has not been possible to perform experiments in 2D flow, because a new wind tunnel model with two end-plates, as well as a different experimental set-up would have been necessary. However, on the basis of the results obtained, it is inferred that the bistable flow disappears in 2D conditions (Chapter Chapter 8).

5.5 Effect on wind load

In the tip region, where the asymmetric flow is particularly apparent in SR1 (Figure 5.37), the steady lift is enhanced by high suction on the bubble side (that is, in any case, comparable to SR0) and the relatively lower suction on the normal side. However, C_L remains in any case relatively low (about 0.2-0.3), and the resulting bending moment in the cross-wind direction is not significantly high (see section 7.2.2).

The typical second islet of $C_{p,min}$ in the wake of the cylinder (see e.g. Figure 3.23, Figure 3.24, Figure 3.25, Figure 3.29), produced – according to Kawamura et al. (1984) – by the attachment of trailing swirls, is clear in SR0, but it cannot be detected in SR1 (Figure 5.37a). Such a minimum pressure islet in the tip region is responsible, on free-end cylinders, for the increase in drag in the tip region. Therefore, the tip effect is less pronounced in presence of rings (Figure 5.39). Instead, along the height, the drag coefficient is higher in SR1 than in SR0, due to the separation bubble in the wake, as proved by the mean pressure distribution at 650 mm in Figure 5.38.

On the normal side of the cylinder at middle height the mean and rms distributions of C_p (averaged within only one state) resemble the corresponding distributions in absence of rings. On the bubble side, the negative mean pressures decrease after 90° and this increases the drag force. Also the rms values increase on the bubble side. The effect on the response is quantified in sections 7.2.2 and 7.3.4.

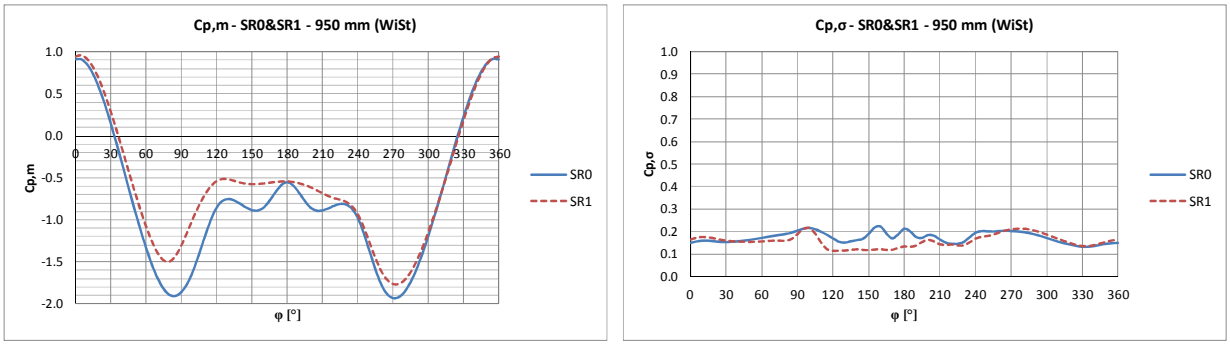

a) *b)*

Figure 5.37 $C_{p,m}$ (a) and $C_{p,\sigma}$ (b) in the tip region with and without rings (WiSt, T1-SR0/SR1-R1-EF0)

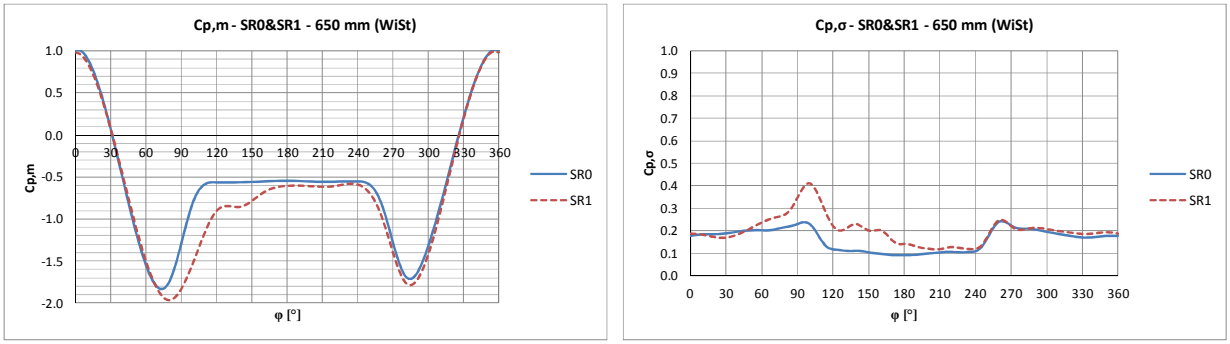

a) *b)*

Figure 5.38 $C_{p,m}$ (a) and $C_{p,\sigma}$ (b) at middle height with and without rings (WiSt, T1-SR0/SR1-R1-EF0)

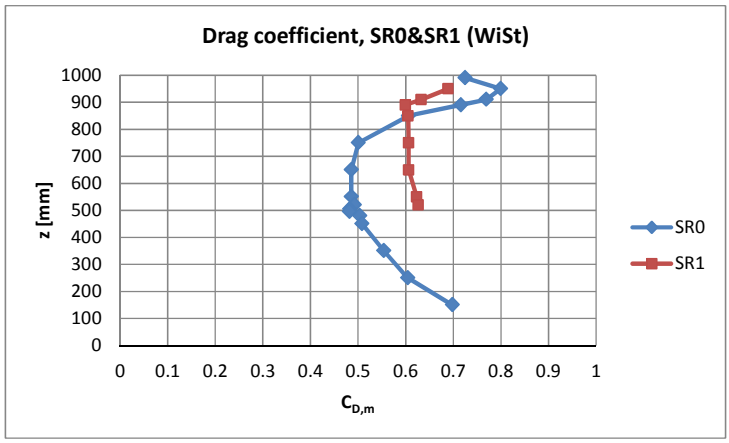

Figure 5.39 $C_{D,m}$ with and without rings (WiSt, T1-SR0/SR1-R1-EF0)

Measurements at low levels (z/H < 0.5) are not available in case of rings at WiSt. However, in order to figure out a three-dimensional distribution of the asymmetric load, the same behaviour as in Figure 5.38 is also hypothesized at lower levels so that, in practice, the presence of rings increases the load on the bubble side. Figure 5.40 and Figure 5.41 plot the resulting $C_{p,m}$ and $C_{p,\sigma}$ distributions, respectively. They are idealized distributions on the safe side, because the two states tend to be mixed as the height decreases (Figure 6.12).

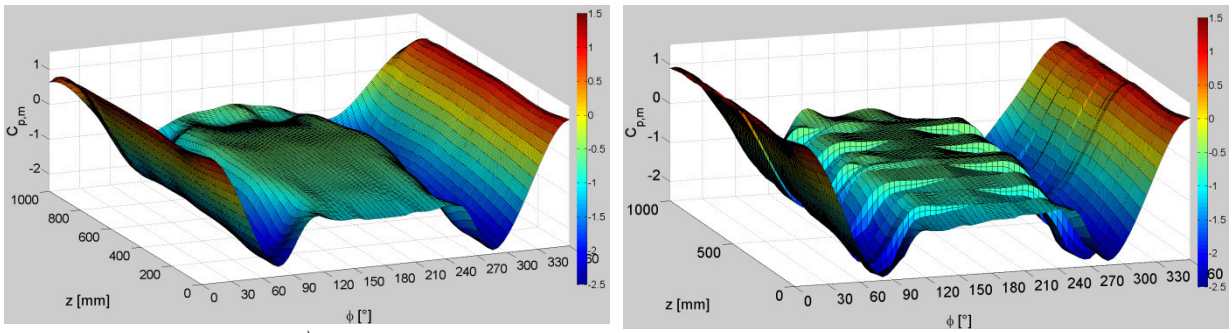

a) *b)*

Figure 5.40 $C_{p,m}$ on the tower: a) without rings; b) with 10 rings (WiSt, T1-SR0/SR1 -R1-EF0)

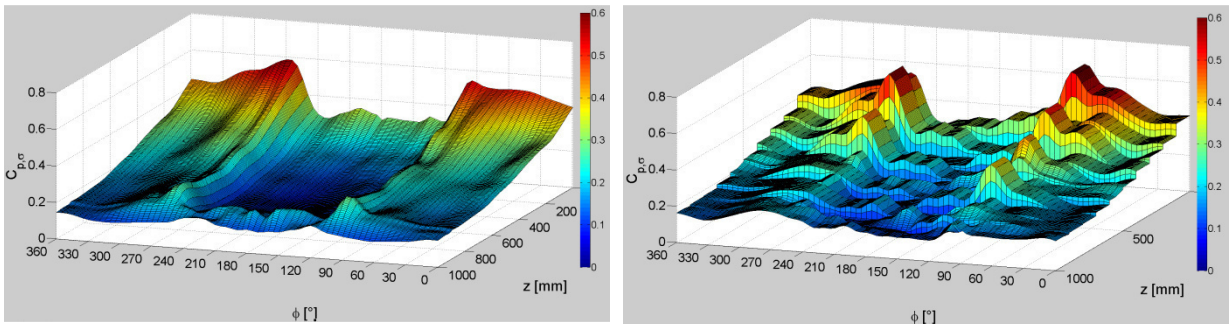

a) *b)*

Figure 5.41 $C_{p,\sigma}$ on the tower: a) without rings; b) with 10 rings (WiSt, T1-SR0/SR1 -R1-EF0)

While in terms of $C_{p,m}$ and $C_{p,\sigma}$ the effect of the rings is a general increase in load, the correlation field is generally reduced.

In terms of horizontal correlations, in case of rings the matrices lose the symmetry with respect to the secondary diagonal, because of the asymmetric conditions between the two sides of the cylinder. Apart from that, the differences are not so relevant. The level z/H = 0.75 is chosen as representative in Figure 5.42, but the same concept applies at the other levels, too. In the case of rings, the correlation field is smoother on the bubble side (180°-360°), where the downstream movement of the separation point, together with the separation bubble, conceal the valley at the separation angle. In the wake, the correlation in case of rings is lower. It consequently decreases the drag force and partly counterbalances the higher Cp_{σ}. However, even though the analysis of the correlation field in SR1 resulted very important for the understanding of the fluid–dynamic phenomenon, structural calculations can safely use the correlation field in SR0 (see Chapter 7).

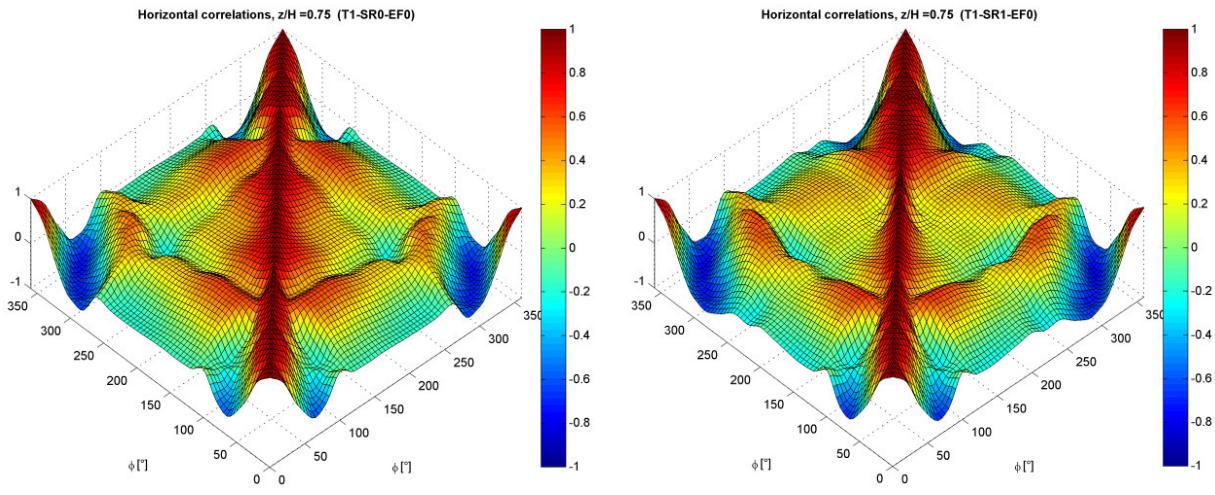

a) *b)*

Figure 5.42 Horizontal correlation field at z/H = 0.75: a) without rings; b) with 10 rings (WiSt, T1-SR0/SR1-R1-EF0)

The vertical cross-correlations are not modified at stagnation and in the frontal region, as motivated in section 5.4. Further downstream, the correlations between levels may show drops in the vicinity of the rings and even at middle levels, as in Figure 5.33. In the wake, there is a reduction of vertical correlations, which is, however, not particularly relevant because the fluctuations in the wake are small.

5.6 Mitigation strategies

After the full investigation, any reason could not be detected which suggested the disappearance of the phenomenon at higher Re. It is then believed – so far, on the basis of this work – that the same phenomenon should also occur in full-scale, whether the same number and size of rings of the experiments are used.

The case of ten big rings, i.e. SR1, represents the upper limit in a design condition. Such big rings may not be necessary. Neverthless, the designer should be aware that an improper use of stiffening rings may produce a negative effect, i.e. the improvement in the structural response can be accompanied by an even more severe load condition.
In the case of rings, the wind load depends on the number, on the size and on the distribution of rings, because different flow structures, like tip-associated vortices and separation bubbles develop in a different way. Therefore, a unified wind load condition for the tower with rings does not exist. The experiments during this work tested several situations and even more are recommended for future research. In chapter 7, a simplified load modelling is provided to the designer. Being unique and being simplified, it cannot include all the load patterns produced by the many different distributions of rings along the height.
Therefore, the aim should be to mitigate, as much as possible, the effect of the rings on the load, in order to design the tower with reference to the design wind load in SR0, that is an established load condition.
Intuitively, small rings at large distance reduce the bistable asymmetric effect. Section 5.3.6 showed that with five rings, even big, the flow is neither bistable nor asymmetric. From the structural point of view, however, it might be preferred to use small rings but more than five. The use of small rings is of course a mitigation strategy, but the tests have shown that e.g. ten rings, even small, still produce an asymmetric flow. In this regard, it is also important to remember that with ten rings, either small or big, the tip-associated vortices are suppressed. Ten rings equally spaced are placed, in this case of study, at a smaller distance than the tower diameter (2/3D). This suggests that a too dense distribution of rings disturbs the tip-associated vortices.

The more pronounced fragmentation of the big vortices on one side of the cylinder produces the not-symmetry, once it is analyzed in the frequency domain. Therefore, rings at a larger distance than one diameter (or, more safely, at 4/3D as it is in SR5) mitigate the effect. If needed, the rings can be placed at larger distance only in the tip region, where the tip-associated vortices are confined.

In any case, it must be remembered that the bistable asymmetric effect is naturally mitigated by the presence of efflux inside the chimney. This is a great advantage, even though out-of-use conditions cannot be neglected.